Open access • Journal Article • DOI:10.1038/S42255-018-0007-6

Interaction between Hormone-Sensitive Lipase and ChREBP in Fat Cells Controls Insulin Sensitivity — Source link

Pauline Morigny, Pauline Morigny, Marianne Houssier, Marianne Houssier ...+77 more authors

Institutions: French Institute of Health and Medical Research, Paul Sabatier University, Centre national de la recherche scientifique, Paris Descartes University ...+14 more institutions

Published on: 01 Jan 2019

Topics: Insulin receptor, Insulin resistance, Insulin, Hormone-sensitive lipase and Adipose tissue

Interaction between Hormone-Sensitive Lipase and ChREBP in Fat Cells Controls Insulin Sensitivity

Pauline Morigny, Marianne Houssier, Aline Mairal, Claire Ghilain, Etienne Mouisel, Fadila Benhamed, Bernard Masri, Emeline Recazens, Pierre-Damien Denechaud, Geneviève Tavernier, et al.

Interaction between Hormone-Sensitive Lipase and ChREBP in Fat Cells Controls Insulin Sensitivity

Pauline Morigny[1,2,26], Marianne Houssier[1,2,26], Aline Mairal[1,2], Claire Ghilain[1,2], Etienne Mouisel[1,2], Fadila Benhamed[3,4,5], Bernard Masri[1,2], Emeline Recazens[1,2], Pierre-Damien Denechaud[1,2], Geneviève Tavernier[1,2], Sylvie Caspar-Bauguil[1,2,6], Sam Virtue[7], Veronika Sramkova[1,2,8,9], Laurent Monbrun[1,2], Anne Mazars[1,2], Madjid Zanoun[1,2], Sandra Guilmeau[3,4,5], Valentin Barquissau[1,2], Diane Beuzelin[1,2], Sophie Bonnel[1,2,9], Marie Marques[1,2,9], Boris Monge-Roffarello[1,2], Corinne Lefort[1,2], Barbara Fielding[10], Thierry Sulpice[11], Arne Astrup[12], Bernard Payrastre[1,2], Justine Bertrand-Michel[1,2], Emmanuelle Meugnier[13], Laetitia Ligat[14], Frédéric Lopez[14], Hervé Guillou[15,16], Charlotte Ling[17], Cecilia Holm[18], Remi Rabasa-Lhoret[19,20,21], Wim H. M. Saris[22], Vladimir Stich[8,9], Peter Arner[23], Mikael Rydén[23], Cedric Moro[1,2,9], Nathalie Viguerie[1,2,9], Matthew Harms[24], Stefan Hallén[24], Antonio Vidal-Puig[7,25], Hubert Vidal[13], Catherine Postic[3,4,5], Dominique Langin[1,2,6,9*]

[1] Institut National de la Santé et de la Recherche Médicale (Inserm), UMR1048, Institute of Metabolic and Cardiovascular Diseases, Toulouse, France;

[2] University of Toulouse, UMR1048, Institute of Metabolic and Cardiovascular Diseases, Paul Sabatier University, Toulouse, France;

[3] Institut National de la Santé et de la Recherche Médicale (Inserm), U1016, Institut Cochin, Paris, France;

[4] Centre National de la Recherche Scientifique (CNRS), UMR 8104, Paris, France;

[5] Université Paris Descartes, Sorbonne Paris Cité, Paris, France;

[6] Toulouse University Hospitals, Laboratory of Clinical Biochemistry, Toulouse, France;

[7] University of Cambridge Metabolic Research Laboratories, Wellcome Trust-MRC Institute of Metabolic Science, Addenbrooke's Hospital, Cambridge CB2 0QQ, UK;

[8] Department for the Study of Obesity and Diabetes, Third Faculty of Medicine, Charles University, Prague, Czech Republic;

[9] Franco-Czech Laboratory for Clinical Research on Obesity, Third Faculty of Medicine, Prague and Paul Sabatier University, Toulouse, France;

[10] Department of Nutritional Sciences, University of Surrey, Guildford, Surrey;

[11] Physiogenex SAS, Prologue Biotech, Labège, France;

[12] Department of Nutrition, Exercise and Sports, Faculty of Science, University of Copenhagen, Copenhagen, Denmark;

[13] CarMeN Laboratory, Inserm U1060, INRA U1397, Université Lyon 1, INSA Lyon, Oullins, France;

[14] Pôle Technologique, Cancer Research Center of Toulouse (CRCT), Plateau Interactions Moléculaires, INSERM-UMR1037, 31037 Toulouse, France.

[15] Institut National de la Recherche Agronomique (INRA), UMR1331, Integrative Toxicology and Metabolism, Toulouse, France

[16] University of Toulouse, UMR1331, Institut National Polytechnique (INP), Paul Sabatier University, Toulouse, France;

[17] Department of Clinical Sciences, Epigenetics and Diabetes, Lund University Diabetes Centre, Clinical Research Centre, Malmö, Sweden;

[18] Department of Experimental Medical Science, Lund University, Biomedical Centre, Lund, Sweden;

[19] Institut de Recherches Cliniques de Montréal, Montreal, Canada;

[20] Department of nutrition, Université de Montréal, Montreal, Canada;

[21] Montreal Diabetes Research Center (MDRC), Montreal, Canada;

[22] Department of Human Biology, NUTRIM School of Nutrition and Translational Research in Metabolism, Maastricht University Medical Centre, Maastricht, Netherlands;

[23] Department of Medicine, H7 Karolinska Institutet and Karolinska University Hospital, Huddinge, Stockholm, Sweden;

[24] Cardiovascular, Renal and Metabolism, IMED Biotech Unit, AstraZeneca, Gothenburg, Sweden;

[25] Wellcome Trust Sanger Institute, Wellcome Trust Genome Campus, Hinxton, Cambridgeshire CB10 1SA, UK;

[26] These authors contributed equally to the work.

*e-mail : dominique.langin@inserm.fr

ABSTRACT

Impaired adipose tissue insulin signaling is a critical feature of insulin resistance. Here we identify a pathway linking the lipolytic enzyme, hormone-sensitive lipase (HSL), to insulin action via the glucose-responsive transcription factor ChREBP and its target, the fatty acid (FA) elongase, ELOVL6. Genetic inhibition of HSL in human adipocytes and mouse adipose tissue results in enhanced insulin sensitivity and induction of ELOVL6. ELOVL6 promotes an increase in phospholipid (PL) oleic acid which modifies plasma membrane fluidity and enhances insulin signaling. HSL deficiency-mediated effects are suppressed by gene silencing of ChREBP and ELOVL6. Mechanistically, physical interaction between HSL and ChREBPα, independently of lipase catalytic activity, impairs ChREBPα translocation into the nucleus and induction of ChREBPβ, the transcriptionally highly active isoform strongly associated to whole body insulin sensitivity. Targeting the HSL-ChREBP interaction may allow therapeutic strategies for the restoration of insulin sensitivity.

Introduction

Insulin resistance is a pathogenic mechanism involved in a wide array of diseases. Besides the well-established early defect seen in type 2 diabetes, insulin resistance plays a role in the development of cancers such as colorectal cancer, liver diseases associated with non-alcoholic steatohepatitis, cardiovascular diseases or, reproductive dysfunction e.g., in polycystic ovary syndrome. Insulin resistance is also a feature of aging-related disorders such as neurodegenerative diseases e.g., in Alzheimer disease. Adipose tissue metabolism has emerged as a major determinant of systemic insulin sensitivity. Genetic ablation of insulin-induced glucose transport in fat causes systemic insulin resistance [1]. Direct manipulation of the fat cell insulin signaling pathway in mice also supports the systemic importance of adipose tissue [2-4]. Defects in adipose insulin signaling have been reported in insulin resistant and type 2 diabetic patients [5-8]. In this context, improvement of adipose tissue insulin action appears to be an important target for recovery of whole body systemic insulin sensitivity. Glitazones, a well-known class of insulin sensitizers, act through modulation of fat cell insulin sensitivity [9,10]. Given their side-effects and subsequent withdrawal in many countries, there is an unmet need of drugs targeting adipose tissue. Excessive circulating levels of fatty acids are considered as important contributors to insulin resistance through development of fatty acid-induced lipotoxicity in insulin-sensitive tissues such as liver and skeletal muscle [11]. Lowering of plasma non-esterified fatty acid levels through inhibition of fat cell lipolysis has been proposed as an approach to improve insulin sensitivity. However, human data questions the association between production of fatty acids from adipose tissue lipolysis and insulin resistance in obesity [12]. Partial deficiency in HSL (encoded by *LIPE*), one of the neutral lipases expressed in adipocytes, results in improvement of whole body insulin sensitivity in obese mice without changes in plasma fatty acid levels suggesting that other mechanisms than lipolysis are involved [13].

Here, in a series of in vitro and in vivo studies in humans and mice, we identified a pathway linking HSL to insulin resistance through interaction with the glucose-responsive transcription factor ChREBP. The physical interaction between HSL and ChREBP impairs nuclear translocation and activity of the transcription factor. In fat cells, the lipogenic enzyme ELOVL6 is a preferential target of ChREBP. Inhibition of HSL promotes activity of ELOVL6 and enhances insulin signaling through enrichment of plasma membrane phospholipids in oleic acid.

Reduction in HSL expression promotes *de novo* lipogenesis and insulin signaling in human adipocytes

In adipocytes differentiated from human multipotent adipose-derived stem (hMADS) cells [14,15], HSL gene silencing (**Supplementary Fig. 1a,b,c**) increased insulin-stimulated glucose transport (**Fig. 1a**), glucose oxidation (**Fig. 1b**) and glucose carbon incorporation into FA, i.e. *de novo* lipogenesis (**Fig. 1c**). Insulin signaling was enhanced in adipocytes with decreased HSL expression as shown by enhanced activating phosphorylations of insulin receptor substrate 1 (IRS1-pY612) and V-Akt murine thymoma viral oncogene homolog (AKT)/protein kinase B (AKT-pS473, AKT-pT308) after insulin treatment (**Fig. 1d,e,f**). Phosphorylation of AS160, an AKT substrate regulating translocation of the insulin-sensitive glucose transporter GLUT4, showed a trend similar to IRS1 and AKT phosphorylation (**Fig. 1g**). As adipose tissue *de novo* lipogenesis is associated with insulin sensitivity in humans [16,17], we tested whether direct inhibition of *de novo* lipogenesis has an impact on the modulation of insulin signaling induced by HSL depletion. To this end, human adipocytes were treated with a selective inhibitor of FA synthase, the rate-limiting enzyme in the synthesis of palmitic acid (**Supplementary Fig. 1d**). The FA synthase inhibitor blunted the induction of insulin-mediated phosphorylation of AKT observed in HSL-deficient fat cells

(**Supplementary Fig. 1e**). To further probe the role of *de novo* lipogenesis, we analyzed FA composition in fat cell triglycerides (TG) and PL. HSL inhibition significantly decreased the proportion of palmitic acid and palmitoleic acid but increased that of oleic acid in TG and PL (**Fig. 1h,i**).

To define the molecular mechanisms underlying the changes in FA composition, we analyzed gene expression of enzymes catalyzing key steps in the synthesis of the main saturated and monounsaturated FA derived from glucose in human fat cells (**Supplementary Fig. 1d**). In hMADS adipocytes with decreased HSL expression, the most robust induction was observed for *ELOVL6* (**Fig. 1j**). The increase in *ELOVL6* mRNA level was mirrored by an increase in enzyme activity (**Supplementary Fig. 1f**) and an increase in the FA elongation ratio attributable to ELOVL6 activity (**Supplementary Fig. 1g**). To confirm data from hMADS adipocytes, we performed HSL gene silencing in human preadipocytes differentiated in primary cultures. *ELOVL6* also showed the highest induction among *de novo* lipogenesis genes (**Supplementary Fig. 1h**). Next, we evaluated the effect of adipose triglyceride lipase (ATGL encoded by *PNPLA2*), through ATGL gene silencing in hMADS adipocytes (**Supplementary Fig. 1i,j**). ATGL precedes HSL in the sequential breakdown of TG during adipocyte lipolysis. Contrarily to what is observed during HSL depletion, ATGL knock down had no effect on *ELOVL6* and other *de novo* lipogenic enzyme mRNA levels as well as on the FA elongation ratio attributable to ELOVL6 activity (**Supplementary Fig. 1k,l**). Altogether, the results show that HSL depletion improves insulin signaling and, promotes *de novo* lipogenesis and modification in FA composition. These changes are associated with induction of the FA elongase ELOVL6.

HSL inhibition is associated with improved insulin sensitivity and increased adipose tissue *Elovl6* expression in vivo

To probe changes in insulin sensitivity upon decreased HSL expression in vivo, we investigated different mouse transgenic models, genetic backgrounds and diets. First, we investigated B6D2/F1 transgenic mice with *Lipe* haploinsufficiency fed with 60% high fat diet [13]. Compared to obese wild type littermates, the mice showed no differences in body weight and fat mass (**Supplementary Fig. 2a,b**). During euglycemic hyperinsulinemic clamp, the glucose infusion rate tended to increase (**Fig. 2a**) while there was no change in glucose rate of disappearance in obese *Lipe* haploinsufficient mice compared with wild type littermates (**Fig. 2b**). Insulin-mediated suppression of hepatic glucose production was improved (**Fig. 2c**). In a second cohort of B6D2/F1 mice fed 45% high fat diet, insulin tolerance was improved while body weight was not modified in *Lipe* haploinsufficient mice compared with wild type littermates (**Fig. 2d, Supplementary Fig. 2c**). In a third cohort of C57BL/6J mice fed 60% high fat diet, we confirmed enhanced insulin sensitivity in *Lipe* haploinsufficient mice as determined by quantitative insulin-sensitivity check index (QUICKI) (**Fig. 2e**). Adipose *Elovl6* gene expression was higher in mice with diminished HSL expression (**Fig. 2f**). As in human adipocytes (**Fig. 1j, Supplementary Fig 1h**), the induction was more pronounced for *Elovl6* than for other lipogenic genes (**Supplementary Fig. 2d**).

To generate a mouse model with HSL knock down in adipose tissue and unaltered expression in liver, we produced B6D2/F1 mice with zinc finger nuclease-mediated deletion of exon B (**Supplementary Fig. 2e**). The promoter upstream of exon B governs HSL expression in fat cells [18]. $Lipe^{exonB-/-}$ mice showed decreased expression of HSL in adipose tissue (**Fig. 2g,h**). In liver, the low levels of HSL which are mainly composed of exon A-containing transcripts, were not modified (**Supplementary Fig. 2f,g**). $Lipe^{exonB-/-}$ mice fed high fat diet showed improved glucose tolerance (**Fig. 2i**) without alteration of body weight (**Supplementary Fig. 2h**). Adipose *Elovl6* gene expression was higher in these mice compared to wild type

littermates (**Fig. 2j**). Pharmacological inhibition of HSL had positive effect in C57BL/6J mice. Chronic treatment with a specific inhibitor of HSL did not alter body weight (**Supplementary Fig. 2i**) but resulted in increased QUICKI (**Supplementary Fig. 2j**) and higher induction of adipose *Elovl6* gene expression (**Supplementary Fig. 2k**). Therefore, both genetic and pharmacologic inhibition of HSL results in improved insulin sensitivity and enhanced *Elovl6* expression in adipose tissue in vivo.

Adipose ELOVL6 has a positive effect on insulin signaling and is associated with insulin sensitivity in vitro and in vivo

To determine whether ELOVL6 was involved in the improvement of insulin signaling when fat cell HSL expression is diminished, we performed siRNA-mediated knockdown of ELOVL6 in human adipocytes. Gene silencing led to a significant decrease in *ELOVL6* mRNA level and activity (**Supplementary Fig. 3a,b**). The increases in IRS1 (**Fig. 3a**) and AKT (**Fig. 3b, Supplementary Fig. 3c**) phosphorylation observed in HSL-deficient adipocytes were abrogated following concomitant gene silencing of ELOVL6. To assess the importance of Elovl6 on adipose tissue insulin signaling in vivo, a bolus of insulin was injected to wild type and *Elovl6* null mice of similar body weights prior to collection and analyses of fat pads (**Supplementary Fig. 3d,e**). In agreement with in vitro data in human adipocytes, insulin-stimulated Akt phosphorylation was decreased in adipose tissue of *Elovl6* null mice (**Fig. 3c**). These results reveal a strong link between ELOVL6 and insulin signaling in fat cells and identify ELOVL6 as the mediator of the beneficial effects of HSL inhibition.

The relationship between adipose tissue ELOVL6 and insulin sensitivity was further explored in mouse models and clinical cohorts. In mice fed high fat diet, the C57BL/6J strain showed higher insulin tolerance than DBA/2J strain (**Fig. 3d, Supplementary Fig. 3f**). The better insulin action in C57BL/6J mice was accompanied by higher induction of adipose tissue *Elovl6* gene expression during refeeding (**Fig. 3e**). In humans, *ELOVL6* gene expression was

first measured in visceral adipose tissue from lean insulin-sensitive individuals and obese patients with metabolic syndrome, the latter being characterized by higher body mass index and lower glucose disposal rate measured during euglycemic hyperinsulinemic clamp (**Fig. 3f, Supplementary Fig. 3g**). Adipose tissue *ELOVL6* mRNA levels were lower in insulin resistant individuals (**Fig. 3g**). Additional evidence was provided by a longitudinal study. In morbidly obese subjects, the weight loss observed two years after bariatric surgery (**Supplementary Fig. 3h**) was associated with an improvement in insulin sensitivity estimated by euglycemic hyperinsulinemic clamp-derived M value (**Fig. 3h**) and an increase in subcutaneous adipose *ELOVL6* mRNA level (**Fig. 3i**). A strong positive correlation was found between *ELOVL6* mRNA levels in subcutaneous fat and M value (**Supplementary Fig. 3i**). Taken together, both murine and human data show a positive association between adipose *ELOVL6* expression and insulin sensitivity in vivo.

ELOVL6 positive effect on insulin signaling is mediated by oleic acid content in PL and plasma membrane fluidity

We sought to identify the mechanisms by which ELOVL6 improves insulin signaling. Considering that the enzyme catalyzes critical steps in FA synthesis (**Supplementary Fig. 1d**), we investigated the direct contribution of ELOVL6 on the changes in fat cell FA composition. In TG (**Fig. 4a**) and PL (**Fig. 4b**) of human adipocytes, diminished ELOVL6 expression led to an increase in palmitic acid and palmitoleic acid at the expense of oleic acid. Analyses of these FAs were then performed on each class of PL. ELOVL6-deficient adipocytes showed a decrease in the proportion of oleic acid (e.g., 36:2) and an increase in the proportion of palmitic acid (e.g., 32:0) and palmitoleic acid (e.g., 32:2) in phosphatidylcholines and phosphatidylethanolamines (**Supplementary Fig. 4a-d**). In phosphatidylinositides, there was a decrease in 36:2 whereas no change was observed for

phosphatidylserines. These findings were in agreement with in vivo data, where the lack of *Elovl6* in mouse adipose tissue resulted in increased palmitic and palmitoleic acid and decreased oleic acid contents in adipose tissue (**Supplementary Fig. 4e**). The changes in FA composition of PL suggest potential modification in plasma membrane properties. As ELOVL6 mediates the positive effect of HSL gene silencing on insulin signaling (**Fig. 3a,b, Supplementary Fig. 3c**), we determined whether this effect was dependent on oleic acid. There are two enzymatic steps between palmitic acid and oleic acid (**Supplementary Fig. 1d**). The first is the elongation of palmitic acid into stearic acid catalyzed by ELOVL6 and the second is the desaturation of stearic acid into oleic acid catalyzed by SCD, a highly active process in fat cells [19-22]. To investigate the respective contribution of the two steps, specific inhibitors were used. Treatment of human adipocytes with an inhibitor of ELOVL6 [23] resulted in the expected changes in FA composition with a decrease of the C18/C16 FA ratio (**Fig. 4c**). Concordant with data obtained using gene silencing (**Fig. 3b**), pharmacological inhibition of ELOVL6 abrogated the enhancement of insulin-induced AKT phosphorylation observed in HSL-deficient adipocytes (**Fig. 4d**). A specific SCD inhibitor [24] decreased C16 and C18 FA desaturation (**Fig. 4e**) and had the same effect as the ELOVL6 inhibitor on AKT phosphorylation (**Fig. 4f**). Our data suggest that SCD is necessary but does not play a rate-limiting role as does ELOVL6 in the improvement of insulin signaling induced by HSL inhibition. Accordingly, *SCD* mRNA levels are much higher than *ELOVL6* mRNA levels in human adipocytes (**Supplementary Fig. 4f**). In additional experiments, the content of oleic acid in PL was directly modified by incubation of adipocytes with the FA (**Fig. 4g**). Exposure of HSL and ELOVL6 double deficient adipocytes to oleic acid rescued insulin-induced AKT phosphorylation to levels comparable with that observed in fat cells with diminished HSL expression (**Fig. 4h**). Therefore, the beneficial role of ELOVL6 on insulin signaling in human adipocytes is mediated by modulation of oleic acid content.

The composition of FA in PL may influence insulin signal transduction through modification of plasma membrane properties [19,25,26]. To determine the consequence of ELOVL6-mediated changes in PL FA composition on plasma membrane fluidity, overexpression of ELOVL6 in human adipocytes was achieved using an adenoviral vector (**Supplementary Fig. 4g,h**). The resulting increase in C18/C16 FA ratio (**Fig. 4i**) was associated with an increase in insulin-induced IRS1 phosphorylation (**Fig. 4j**). Fluorescence recovery after photobleaching (FRAP) data were analyzed in cells overexpressing ELOVL6 which plasma membrane glycolipids were labeled by fluorescent cholera toxin subunit B (**Fig. 4k**). Comparison of the mobile fractions (**Fig. 4l**) revealed an increase in plasma membrane lateral mobility of cholera toxin-bound glycolipids in ELOVL6-overexpressing adipocytes. Collectively, the data suggest that enhanced adipocyte ELOVL6 activity increases the proportion of oleic acid in PL and positively influences insulin signaling through modulation of plasma membrane fluidity.

The glucose-responsive transcription factor ChREBP mediates the beneficial effect of diminished HSL expression through ELOVL6 induction

ELOVL6 is a direct transcriptional target of ChREBP [27]. Adipose ChREBP is a major determinant of systemic insulin action on glucose metabolism [28]. Therefore, the direct contribution of ChREBP to HSL gene silencing-mediated improvement of glucose metabolism in human adipocytes was evaluated using RNA interference (**Supplementary Fig. 5a**). During dual knockdown of HSL and ChREBP, the beneficial effects on glucose metabolism observed in adipocytes with low HSL expression were diminished. Glucose transport was decreased to control levels and the induction of *de novo* lipogenesis observed in cells with single HSL knockdown was lowered in adipocytes with dual knockdown of HSL and ChREBP (**Fig. 5a,b**). A similar pattern was observed for glucose and acetate carbon incorporation into FA (**Fig. 5b,c**) showing that the upregulation of FA synthesis resulted not

only from increased glucose uptake but also from specific induction of *de novo* lipogenesis. ChREBP gene silencing also mitigated the increase in insulin-induced IRS1 and AKT phosphorylation (**Fig. 5d,e**). These results indicate that ChREBP is involved in the improvement of glucose metabolism and insulin signaling induced by HSL downregulation. Similarly to what had been observed for ELOVL6 knock down (**Fig. 4a,b**), ChREBP gene silencing led to an increase in palmitic acid and palmitoleic acid and a decrease of oleic acid (**Fig. 5f,g**). Accordingly, ChREBP gene silencing potently suppressed *ELOVL6* gene expression but had weak or no effect on other lipogenic genes suggesting that ELOVL6 is a preferential target of ChREBP in human fat cells (**Fig. 5h**). The involvement of ChREBP in adipose *Elovl6* gene expression was confirmed in vivo. In adipose tissue of *Mlxipl* null mice (**Supplementary Fig. 5b**), *Elovl6* was the lipogenic gene which expression was the most severely impaired (**Fig. 5i**).

Two isoforms of ChREBP have been identified. ChREBPα, which transcriptional activity is regulated by glucose, and ChREBPβ, a transcriptionally superactive and unstable isoform which is a direct transcriptional target of ChREBPα [28,29]. We characterized the human β-specific exon of *MLXIPL* which extends 29 deoxynucleotides 3' of its mouse counterpart [28] (**Supplementary Fig. 5c**). In human adipocytes with siRNA-mediated knock down of HSL, the levels of *ChREBP* transcripts, notably the β isoform, were increased (**Fig. 5j**). Recruitment of ChREBP on the functional carbohydrate response element (ChoRE) in the *ELOVL6* promoter was investigated using chromatin immunoprecipitation assays [27]. In hMADS adipocytes, more binding events were detected on the *ELOVL6* ChoRE than on positive control regions in *RORC* and *TXNIP*, a well characterized target of ChREBP (**Supplementary Fig. 5d**). ChREBP recruitment onto the *ELOVL6* promoter was markedly enhanced in HSL-deficient compared to control adipocytes (**Fig. 5k**).

Interestingly, *ELOVL6* was strongly associated with *ChREBPβ* gene expression in human hMADS adipocytes (**Fig. 5l**) and human differentiated primary preadipocytes (**Supplementary Fig. 5e**). Albeit less potent, a positive correlation was also found between *ELOVL6* and *ChREBPα* (**Supplementary Fig. 5f**). Similarly, a highly significant correlation between *ELOVL6* and *ChREBPβ* was observed in human subcutaneous adipose tissue samples (**Fig. 5m**). Short term elevation in plasma glucose and insulin levels during a hyperglycemic hyperinsulinemic clamp led to a pronounced induction of adipose *ChREBPβ* (**Fig. 5n**) and *ELOVL6* (**Fig. 5o**) gene expression, illustrating the importance of glucose flux into the fat cells in the control of *ELOVL6* expression in humans. Altogether, our results show that ChREBPβ mediates the effect of HSL deficiency on glucose metabolism and insulin signaling through transcriptional activation of *ELOVL6*.

HSL modifies ChREBP activity in fat cells through protein-protein interaction

As HSL catalyzes one of the rate-limiting steps in fat cell TG hydrolysis, we investigated whether lipolysis per se contributed to the induction of ChREBP. Several lines of evidence suggest that this is not the case. In the culture conditions used to study *de novo* lipogenesis, the release of glycerol and FA in the culture medium was low and was not influenced by HSL gene silencing (**Supplementary Fig. 6a,b**). Adipocytes were then treated with triacsin C, a potent inhibitor of long chain fatty acyl CoA synthetase [14]. If FAs were involved, enhanced FA levels due to blockade of FA re-esterification should influence *ChREBP* and *ELOVL6* induction in adipocytes with HSL knock down. However, the upregulation of *ChREBP* isoform and *ELOVL6* mRNA was not influenced by the treatment (**Supplementary Fig. 6c-e**). These data show that the lipolytic activity of HSL does not contribute to the induction of ChREBP.

These findings led us to hypothesize that physical interaction between HSL and ChREBP may influence ChREBP activity. HEK293 cells were transfected with vectors expressing HSL and ChREBPα with FLAG epitope tag [30]. Immunoprecipitation of cell lysates with anti-FLAG IgG and immunoblotting with anti-HSL antibody showed that HSL co-immunoprecipitated with ChREBPα (**Supplementary Fig. 6f**). Co-immunoprecipitation was observed using FLAG-ChREBP immobilized on magnetic beads and recombinant HSL (**Fig. 6a**). Surface plasmon resonance assays supported a direct binding between ChREBPα and HSL (**Fig. 6b**). Interaction between endogenous proteins in adipocytes was shown through immunoprecipitation with anti-ChREBP and anti-HSL antibodies (**Fig. 6c, Supplementary Fig. 6g**). In line with the lack of effect on *de novo* lipogenesis (**Supplementary Fig. 1k,l**), ATGL displayed no interaction with ChREBPα further indicating that HSL interaction with ChREBPα is independent lipolysis and specific to this neutral lipase (**Fig. 6c**).

Furthermore, interaction of HSL with ChREBPα was shown using in situ proximity ligation assays using a pair of primary antibodies raised in two different species and a pair of secondary antibodies coupled to oligodeoxynucleotides [31]. Specific and robust fluorescence signals were observed in the cytosol of fat cells from subcutaneous adipose tissue (**Supplementary Fig. 6h**). Such signals were also seen in differentiated hMADS adipocytes (**Supplementary Fig. 6i**). Little signal was detected in undifferentiated fibroblasts which do not express HSL. Negative controls using incomplete sets of antibodies and assays using anti-ATGL and anti-AKT combined with anti-ChREBP antibodies supported specificity of the interaction (**Supplementary Fig. 6j,k**). Human HepG2 hepatocytes which express significant level of ChREBP but minute amounts of HSL showed few fluorescent spots (**Supplementary Fig. 6l,m**). Respective expression of ChREBPα and HSL in mouse tissues is coherent with a fat-specific interaction of the two proteins (**Supplementary Fig. 6n**). The data suggest that ChREBPα interaction with HSL is specific to fat cells.

In mouse adipose tissue, co-immunoprecipitation between HSL and ChREBP was diminished in *Lipe* haploinsufficient mice (**Fig. 6d**). In human adipocytes, HSL binding to ChREBPα was reduced in cytoplasm when HSL expression was diminished using siRNA (**Fig. 6e, Supplementary Fig. 7a**). This resulted in modification of ChREBP cellular distribution. Compared to control cells, adipocytes with low HSL expression showed higher immunofluorescence of ChREBP in nuclei indicating that ChREBPα nuclear translocation is facilitated when interaction with HSL is diminished (**Fig. 6f**). Subcellular fractionation confirmed an increased nuclear translocation in human adipocytes and mouse adipose tissues with low HSL expression whereas no significant differences was observed in the cytosolic fraction (**Fig. 6g,h, Supplementary Fig. 7b,c**). In mice, there was no difference in ChREBPα protein content in fat pads of the two genotypes (**Supplementary Fig. 7d**). To evaluate the effect of HSL on ChREBPα transcriptional activity, HEK293 cells were transfected with a vector containing the luciferase reporter gene under the control of a promoter containing functional ChoREs [32]. Promoter activity increased when cells expressed ChREBPα and decreased when cells co-expressed increasing amounts of HSL (**Fig. 6i, Supplementary Fig. 7e**). The data suggest that HSL binds to ChREBPα and sequesters the transcription factor in the cytoplasm. Upon decrease of HSL expression, HSL-ChREBP interaction is diminished, ChREBPα nuclear translocation is facilitated and its transcriptional activity is enhanced as shown here in reporter gene assays and above in chromatin immunoprecipitation analysis (**Fig. 5k**).

When HEK293 cells expressing HSL and ChREBP were treated with a HSL inhibitor, less interaction between HSL and ChREBP was observed (**Supplementary Fig. 7f**). In human adipose tissue, we previously identified a short form of HSL produced by in-frame skipping of exon 6 (**Supplementary Fig. 2e**) [33,34]. As exon 6 encodes the catalytic site Serine, HSL short form is devoid of enzymatic activity (**Supplementary Fig. 7g**). Expressed in HEK293

cells, HSL short form retained the capacity to bind ChREBP (**Fig. 6j**). An adenovirus expressing HSL short form was used to transduce human adipocytes transfected with control or *LIPE* siRNA (**Supplementary Fig. 7h**). The induction of *ELOVL6* in adipocytes with diminished levels of HSL was blunted when HSL short form was expressed (**Fig. 6k**). A similar pattern was observed for other *de novo* lipogenesis gene expression (**Supplementary Fig. 7i**). The catalytically inactive form also reduced the increase in IRS1 phosphorylation mediated by HSL down regulation (**Fig. 6l**). Of note, the improvement of fat cell insulin signaling was observed with no change in amount of ChREBPα protein in adipocytes expressing HSL-S and in the absence of correlation between HSL and ChREBPα levels. (**Supplementary Fig. 7j,k**). Altogether, our data suggest that HSL plays an important role besides the hydrolysis of lipids in fat cells, the repression of ChREBP activity via direct interaction with the transcription factor (**Supplementary Fig. 8**).

Discussion

Considering the soaring incidence of diseases characterized by an insulin resistance state, there is a lack of drugs acting on adipose tissue. Its specialized cells, the adipocytes, have great potential to be therapeutically targeted [35]. Partial inhibition of the fat cell neutral lipase, HSL, alleviates insulin resistance without increasing body weight, two essential requirements for therapeutic interventions [13] (and present work). Evolution of plasma fatty acid level and variation in insulin sensitivity was dissociated in this model. Here, we deciphered the mechanisms behind HSL inhibition-mediated improvement of glucose metabolism and identified interactions between prototypical metabolic pathways of the adipocyte. We show that, independently of lipolysis and the enzyme catalytic activity, HSL physically interacts with and inhibits the transcription factor ChREBP. ChREBP controls the FA elongase ELOVL6 catalyzing a limiting step in oleic acid synthesis. The resulting increase in PL oleic acid content modifies plasma membrane properties and improves insulin signaling.

401 Adipose *de novo* lipogenesis is positively associated with systemic insulin sensitivity [36,37]. *De*
402 *novo* lipogenesis is under the control of the glucose-responsive transcription factor, ChREBP.
403 A positive association between insulin sensitivity and adipose ChREBP, notably, the
404 transcriptionally superactive β isoform, has been reported [16,28,38]. In human adipocytes, we
405 show that knockdown of ChREBP counteracts the beneficial effects of HSL gene silencing on
406 insulin sensitivity. We identify the FA elongase ELOVL6 as the main target of ChREBPβ in
407 HSL-deficient adipocytes. In humans, *ELOVL6* expression in fat was lower in insulin resistant
408 than in insulin sensitive subjects in line with previous reports [16,39]. Of note, in monozygotic
409 twin pairs discordant for type 2 diabetes, adipose *ELOVL6* is markedly lower in the affected
410 twins [40]. Our results from bariatric surgery, a longitudinal intervention improving insulin
411 control of glucose metabolism, also supported the tight link between adipose *ELOVL6* and
412 insulin sensitivity.
413 ELOVL6 catalyzes a critical step in the elongation of C16 FA [22,41]. In adipocytes, enhanced
414 ELOVL6 activity favored oleic acid synthesis while ELOVL6 knock down had the opposite
415 effect. Diets rich in olive oil improve insulin sensitivity at adipocyte and whole-body levels
416 [42,43]. This effect may contribute to the decreased incidence of type 2 diabetes in patients at risk
417 fed Mediterranean diets [43]. At the cellular level, monounsaturated fatty acids have been
418 reported to protect from the damaging effect of palmitic acid on insulin signaling [19,26]. As
419 ELOVL6 induced an increase of oleic acid in major classes of PL, we postulated that it may
420 alter plasma membrane fluidity owing to its conformational plasticity [25,44,45]. The plasma
421 membrane lateral mobility of glycolipids was increased in fat cells overexpressing ELOVL6.
422 We therefore propose that ELOVL6-mediated increase in PL oleic acid content improves fat
423 cell insulin signaling through alteration of plasma membrane properties. In mice, *Elovl6*
424 deficiency impaired white adipose tissue insulin signaling whereas the opposite or lack of

alteration have previously been reported in the liver suggesting tissue-specific differences in ELOVL6-mediated modulation of insulin action [41,46].

The role of HSL in human fat cell lipolysis is well established [14,47]. HSL is a multifunctional enzyme with a broad range of substrates. Besides tri-, di- and monoglycerides, HSL is able to hydrolyze other esters, such as cholesteryl and retinyl esters [48]. As ChREBP activity is influenced by metabolites and other transcription factors in liver, it could be postulated that products of HSL enzymatic activity directly or indirectly influence ChREBP-mediated modulation of gene transcription [29]. However, although we cannot rule out that, in some conditions, upregulation of ChREBPα protein expression partially contributes to the phenotype of adipocytes depleted in HSL, we bring a solid body of evidence that physical interaction between HSL and ChREBPα controls the intracellular location and activity of the transcription factor in fat cells. ATGL which catalyzes the first step in adipose tissue lipolysis does not interact with ChREBP and does not modulate *de novo* lipogenesis gene expression. Moreover, using a short inactive form of HSL lacking the catalytic site Serine, we could show that the catalytic activity of HSL is dispensable for the interaction with ChREBP and ChREBP-mediated effect on *ELOVL6* expression and insulin signaling. Noteworthy, our data provide a function to this naturally occurring form expressed in human adipose tissue [33]. A specific HSL inhibitor was able to diminish the interaction between HSL and ChREBP and enhance adipose *Elovl6* expression in mice. It may be hypothesized that the inhibitor binding to the catalytic pocket induces conformational change partially disrupting HSL-ChREBP interaction. The data suggest that small molecules may be designed and used to disrupt the interaction. Reducing the interaction between HSL and ChREBP favors ChREBP nuclear translocation and its transcriptional activity. This pathway provides a molecular basis to the differential control of *de novo* lipogenesis in liver and adipose tissue. ChREBP is involved in the regulation of *de novo* lipogenesis in the two tissues [29,49]. However, the pathway is

generally considered as detrimental in the liver as it is activated during the development of fatty liver disease whereas it is seen as beneficial in adipose tissue as the link with insulin sensitivity has been shown both in clinical studies and in mouse models [50]. HSL is expressed at much higher level in fat cells than in hepatocytes. Accordingly, interaction between HSL and ChREBP is not found in human hepatocytes. Alleviation of HSL-mediated inhibition of ChREBP activity may constitute a fat cell-specific mechanism to enhance *de novo* lipogenesis and insulin signaling.

To conclude, our work identifies a pathway critical for optimal insulin signaling in fat cells which links the neutral lipase HSL to the glucose-responsive transcription factor ChREBP and its target gene, the FA elongase, ELOVL6. This constitutes a unique example of an enzyme involved in lipid metabolism which independently of its enzymatic activity inhibits the transcriptional activity of a glucose-responsive transcription factor through protein-protein interaction. Inhibition of the HSL-ChREBP interaction may constitute an adipose-specific strategy to reduce insulin resistance.

ACKNOWLEDGMENTS

The authors gratefully acknowledge Dr. Nicolas Venteclef (Centre de Recherche des Cordeliers, Paris, France) and Dr. Jérémie Boucher (AstraZeneca, Göteborg, Sweden) for critical reading and comments on the manuscript. Emilie Courty and Jean Personnaz participated in mouse studies during internship at I2MC. The GenoToul Animal Care, Anexplo, Imaging-TRI (especially, Dr. Frédérique Gaits-Iacovoni for helpful discussion) and Quantitative Transcriptomics facilities contributed to the work.

This work was supported by Inserm, Paul Sabatier University, Fondation pour la Recherche Médicale (DEQ20170336720 to D.L.), Agence Nationale de la Recherche (ANR-12-BSV1-0025Obelip and ANR-17-CE14-0015Hepadialogue to D.L.), Région Midi-Pyrénées (OBELIP and ILIP projects to D.L.), FORCE/F-CRIN for clinical research on obesity, EU/EFPIA Innovative Medicines Initiative Joint Undertaking (EMIF grant n° 115372 to P.A., A.V.P. and D.L.) and AstraZeneca France (TALIP project to D.L.).

D.L. is a member of Institut Universitaire de France.

AUTHOR CONTRIBUTIONS

P.M. and M.H. share first authorship. P.M. and M.Ho. performed the majority of in vitro experiments and analyzed data with the contribution of A.Mai., C.G., F.B., B.M., E.R., P.D.D., V.Sr., V.B., D.B., M.M., C.L., L.L., F.L. and M.Ha. P.M., M.Ho., E.Mo., G.T., S.V., L.M., S.G., B.M.-R., T.S., H.G., C.H., A.V.P. and C.P. performed and analyzed in vivo data from mouse models. P.M., S.B., M.M., B.F., A.A., E.Me., C.L., R.R.L., W.S., V.St., P.A., M.R., N.V. and H.V. performed and analyzed in vivo data in human clinical studies. S.C.-B., S.V. and J.B.-M. analyzed lipidomics data. A.Maz. and M.Z. performed and analyzed FRAP

experiments. B.P., C.M., N.V., S.H. and H.V. interpreted the data. P.M., M.Ho. and D.L. conceived the study, interpreted the data and wrote the manuscript. D.L. supervised the study.

COMPETING INTERESTS STATEMENT

T.S. is an employee of Physiogenex. M.H. and S.H. are employees of AstraZeneca. The other authors declare no competing financial and non-financial interests.

REFERENCES

1. Abel, E.D., *et al.* Adipose-selective targeting of the GLUT4 gene impairs insulin action in muscle and liver. *Nature* **409**, 729-733 (2001).
2. Morley, T.S., Xia, J.Y. & Scherer, P.E. Selective enhancement of insulin sensitivity in the mature adipocyte is sufficient for systemic metabolic improvements. *Nat Commun* **6**, 7906 (2015).
3. Shearin, A.L., Monks, B.R., Seale, P. & Birnbaum, M.J. Lack of AKT in adipocytes causes severe lipodystrophy. *Mol Metab* **5**, 472-479 (2016).
4. Softic, S., *et al.* Lipodystrophy Due to Adipose Tissue Specific Insulin Receptor Knockout Results in Progressive NAFLD. *Diabetes* (2016).
5. Rondinone, C.M., *et al.* Insulin receptor substrate (IRS) 1 is reduced and IRS-2 is the main docking protein for phosphatidylinositol 3-kinase in adipocytes from subjects with non-insulin-dependent diabetes mellitus. *Proc Natl Acad Sci U S A* **94**, 4171-4175 (1997).
6. Carvalho, E., Jansson, P.A., Nagaev, I., Wenthzel, A.M. & Smith, U. Insulin resistance with low cellular IRS-1 expression is also associated with low GLUT4 expression and impaired insulin-stimulated glucose transport. *FASEB J* **15**, 1101-1103 (2001).
7. Frojdo, S., Vidal, H. & Pirola, L. Alterations of insulin signaling in type 2 diabetes: a review of the current evidence from humans. *Biochim Biophys Acta* **1792**, 83-92 (2009).
8. Nyman, E., *et al.* A single mechanism can explain network-wide insulin resistance in adipocytes from obese patients with type 2 diabetes. *J Biol Chem* **289**, 33215-33230 (2014).

9. Hammarstedt, A., Sopasakis, V.R., Gogg, S., Jansson, P.A. & Smith, U. Improved insulin sensitivity and adipose tissue dysregulation after short-term treatment with pioglitazone in non-diabetic, insulin-resistant subjects. *Diabetologia* **48**, 96-104 (2005).

10. Yki-Jarvinen, H. Thiazolidinediones. *N Engl J Med* **351**, 1106-1118 (2004).

11. Samuel, V.T. & Shulman, G.I. Mechanisms for insulin resistance: common threads and missing links. *Cell* **148**, 852-871 (2012).

12. Karpe, F., Dickmann, J.R. & Frayn, K.N. Fatty acids, obesity, and insulin resistance: time for a reevaluation. *Diabetes* **60**, 2441-2449 (2011).

13. Girousse, A.*, et al.* Partial inhibition of adipose tissue lipolysis improves glucose metabolism and insulin sensitivity without alteration of fat mass. *PLoS Biol* **11**, e1001485 (2013).

14. Bezaire, V.*, et al.* Contribution of adipose triglyceride lipase and hormone-sensitive lipase to lipolysis in hMADS adipocytes. *J Biol Chem* **284**, 18282-18291 (2009).

15. Barquissau, V.*, et al.* White-to-brite conversion in human adipocytes promotes metabolic reprogramming towards fatty acid anabolic and catabolic pathways. *Mol Metab* **5**, 352-365 (2016).

16. Eissing, L.*, et al.* De novo lipogenesis in human fat and liver is linked to ChREBP-beta and metabolic health. *Nat Commun* **4**, 1528 (2013).

17. Roberts, R.*, et al.* Markers of de novo lipogenesis in adipose tissue: associations with small adipocytes and insulin sensitivity in humans. *Diabetologia* **52**, 882-890 (2009).

18. Grober, J.*, et al.* Characterization of the promoter of human adipocyte hormone-sensitive lipase. *Biochem J* **328**, 453-461 (1997).

19. Collins, J.M., Neville, M.J., Hoppa, M.B. & Frayn, K.N. De novo lipogenesis and stearoyl-CoA desaturase are coordinately regulated in the human adipocyte and protect against palmitate-induced cell injury. *J Biol Chem* **285**, 6044-6052 (2010).

20. Guillou, H., Zadravec, D., Martin, P.G. & Jacobsson, A. The key roles of elongases and desaturases in mammalian fatty acid metabolism: Insights from transgenic mice. *Prog Lipid Res* **49**, 186-199 (2010).

21. Hodson, L. & Fielding, B.A. Stearoyl-CoA desaturase: rogue or innocent bystander? *Prog Lipid Res* **52**, 15-42 (2013).

22. Ohno, Y.*, et al.* ELOVL1 production of C24 acyl-CoAs is linked to C24 sphingolipid synthesis. *Proc Natl Acad Sci U S A* **107**, 18439-18444 (2010).

23. Nagase, T.*, et al.* Synthesis and biological evaluation of a novel 3-sulfonyl-8-azabicyclo[3.2.1]octane class of long chain fatty acid elongase 6 (ELOVL6) inhibitors. *J Med Chem* **52**, 4111-4114 (2009).

24. Xin, Z.*, et al.* Discovery of piperidine-aryl urea-based stearoyl-CoA desaturase 1 inhibitors. *Bioorg Med Chem Lett* **18**, 4298-4302 (2008).

25. Antonny, B., Vanni, S., Shindou, H. & Ferreira, T. From zero to six double bonds: phospholipid unsaturation and organelle function. *Trends Cell Biol* **25**, 427-436 (2015).

26. Holzer, R.G.*, et al.* Saturated fatty acids induce c-Src clustering within membrane subdomains, leading to JNK activation. *Cell* **147**, 173-184 (2011).

27. Bae, J.S., Oh, A.R., Lee, H.J., Ahn, Y.H. & Cha, J.Y. Hepatic Elovl6 gene expression is regulated by the synergistic action of ChREBP and SREBP-1c. *Biochem Biophys Res Commun* **478**, 1060-1066 (2016).

28. Herman, M.A.*, et al.* A novel ChREBP isoform in adipose tissue regulates systemic glucose metabolism. *Nature* **484**, 333-338 (2012).

568 29. Filhoulaud, G., Guilmeau, S., Dentin, R., Girard, J. & Postic, C. Novel insights into
569 ChREBP regulation and function. *Trends Endocrinol Metab* **24**, 257-268 (2013).
570 30. Stoeckman, A.K., Ma, L. & Towle, H.C. Mlx is the functional heteromeric partner of
571 the carbohydrate response element-binding protein in glucose regulation of lipogenic
572 enzyme genes. *J Biol Chem* **279**, 15662-15669 (2004).
573 31. Soderberg, O.*, et al.* Direct observation of individual endogenous protein complexes in
574 situ by proximity ligation. *Nat Methods* **3**, 995-1000 (2006).
575 32. Lou, D.Q.*, et al.* Chicken ovalbumin upstream promoter-transcription factor II, a new
576 partner of the glucose response element of the L-type pyruvate kinase gene, acts as an
577 inhibitor of the glucose response. *J Biol Chem* **274**, 28385-28394 (1999).
578 33. Laurell, H.*, et al.* Species-specific alternative splicing generates a catalytically inactive
579 form of human hormone-sensitive lipase. *Biochem J* **328 (Pt 1)**, 137-143 (1997).
580 34. Ray, H.*, et al.* The presence of a catalytically inactive form of hormone-sensitive
581 lipase is associated with decreased lipolysis in abdominal subcutaneous adipose tissue
582 of obese subjects. *Diabetes* **52**, 1417-1422 (2003).
583 35. Kusminski, C.M., Bickel, P.E. & Scherer, P.E. Targeting adipose tissue in the
584 treatment of obesity-associated diabetes. *Nat Rev Drug Discov* (2016).
585 36. Czech, M.P. Cellular basis of insulin insensitivity in large rat adipocytes. *J Clin Invest*
586 **57**, 1523-1532 (1976).
587 37. Hoffstedt, J., Forster, D. & Lofgren, P. Impaired subcutaneous adipocyte lipogenesis
588 is associated with systemic insulin resistance and increased apolipoprotein B/AI ratio
589 in men and women. *J Intern Med* **262**, 131-139 (2007).
590 38. Kursawe, R.*, et al.* Decreased transcription of ChREBP-alpha/beta isoforms in
591 abdominal subcutaneous adipose tissue of obese adolescents with prediabetes or early

592 type 2 diabetes: associations with insulin resistance and hyperglycemia. *Diabetes* **62**,
593 837-844 (2013).
594 39. Soronen, J.*, et al.* Adipose tissue gene expression analysis reveals changes in
595 inflammatory, mitochondrial respiratory and lipid metabolic pathways in obese
596 insulin-resistant subjects. *BMC Med Genomics* **5**, 9 (2012).
597 40. Nilsson, E.*, et al.* Altered DNA methylation and differential expression of genes
598 influencing metabolism and inflammation in adipose tissue from subjects with type 2
599 diabetes. *Diabetes* **63**, 2962-2976 (2014).
600 41. Matsuzaka, T.*, et al.* Crucial role of a long-chain fatty acid elongase, Elovl6, in
601 obesity-induced insulin resistance. *Nat Med* **13**, 1193-1202 (2007).
602 42. Ryan, M.*, et al.* Diabetes and the Mediterranean diet: a beneficial effect of oleic acid
603 on insulin sensitivity, adipocyte glucose transport and endothelium-dependent
604 vasoreactivity. *QJM* **93**, 85-91 (2000).
605 43. Salas-Salvado, J.*, et al.* Reduction in the incidence of type 2 diabetes with the
606 Mediterranean diet: results of the PREDIMED-Reus nutrition intervention randomized
607 trial. *Diabetes Care* **34**, 14-19 (2011).
608 44. Ibarguren, M.*, et al.* Partitioning of liquid-ordered/liquid-disordered membrane
609 microdomains induced by the fluidifying effect of 2-hydroxylated fatty acid
610 derivatives. *Biochim Biophys Acta* **1828**, 2553-2563 (2013).
611 45. Pietilainen, K.H.*, et al.* Association of lipidome remodeling in the adipocyte
612 membrane with acquired obesity in humans. *PLoS Biol* **9**, e1000623 (2011).
613 46. Moon, Y.A., Ochoa, C.R., Mitsche, M.A., Hammer, R.E. & Horton, J.D. Deletion of
614 ELOVL6 blocks the synthesis of oleic acid but does not prevent the development of
615 fatty liver or insulin resistance. *J Lipid Res* **55**, 2597-2605 (2014).

616 47. Lafontan, M. & Langin, D. Lipolysis and lipid mobilization in human adipose tissue.
617 *Prog Lipid Res* **48**, 275-297 (2009).
618 48. Kraemer, F.B. & Shen, W.J. Hormone-sensitive lipase: control of intracellular tri-(di-
619)acylglycerol and cholesteryl ester hydrolysis. *J Lipid Res* **43**, 1585-1594 (2002).
620 49. Postic, C. & Girard, J. Contribution of de novo fatty acid synthesis to hepatic steatosis
621 and insulin resistance: lessons from genetically engineered mice. *J Clin Invest* **118**,
622 829-838 (2008).
623 50. Solinas, G., Boren, J. & Dulloo, A.G. De novo lipogenesis in metabolic homeostasis:
624 More friend than foe? *Mol Metab* **4**, 367-377 (2015).
625

FIGURE LEGENDS

Figure 1. Reduced HSL expression promotes glucose metabolism and insulin signaling in human adipocytes. Experiments were carried out in control (white bars, siCTR) and HSL-deprived (grey bars, siHSL) hMADS adipocytes. (**a-g**) Adipocytes were analyzed in basal (-) and insulin-stimulated (+, 100nM) conditions. (**a**) Glucose transport using radiolabelled 2-deoxyglucose (n=12 biologically independent samples per group) (Insulin stimulation: P<0.0001). (**b**) Glucose oxidation using radiolabelled glucose (n=10 biologically independent samples per group) (Insulin stimulation: P=0.0015). (**c**) *de novo* lipogenesis using radiolabelled glucose (n=10 biologically independent samples per group) (Insulin stimulation: P<0.0001). (**d-g**) Insulin signaling evaluated by activating phosphorylation of IRS1 (pY612) (n=7 biologically independent samples per group) (Insulin stimulation: P=0.0033) (**d**) AKT (pS473) (n=5 biologically independent samples per group) (Insulin stimulation: P=0.0005) (**e**), AKT (pT308) (n=8 biologically independent samples per group) (Insulin stimulation: P=0.0201) (**f**) and AS160 (pT642) (n=4 biologically independent samples per group) (Insulin stimulation: P=0.0726) (**g**). Size markers (in kDa) are shown on illustrative Western blot panels. (**h, i**) Fatty acid composition in triglycerides (TG) (**h**) and phospholipids (PL) (**i**) (n=8 biologically independent samples per group). (**j**) mRNA levels of lipogenic enzymes (n=6 biologically independent samples per group). Data are mean ±sem. Statistical analysis was performed using two-way ANOVA with Bonferroni's post hoc tests (**a-g**), paired Student's t test (**h, i**) and Wilcoxon's test (**j**). Statistical tests were two-sided. *P<0.05, **P<0.01, ***P<0.001 compared to control.

Figure 2. HSL inhibition is associated with increased insulin sensitivity and adipose tissue ELOVL6 expression *in vivo.* (**a-f**) Experiments were carried out in wild type (WT, white bars) and HSL haploinsufficient ($Lipe^{+/-}$, grey bars) mice. (**a-c**) Glucose infusion rate (GIR) (**a**) post

651 insulin glucose rate of disappearance (Glucose Rd) (**b**) and hepatic glucose production (HGP)
652 (**c**) during euglycemic-hyperinsulinemic clamp in B6D2/F1 mice fed 60% high fat diet for 3
653 months (WT n=7 animals, *Lipe*$^{+/-}$ n=6 animals). (**d**) Plasma glucose concentration during an
654 insulin tolerance test in B6D2/F1 mice fed 45% high fat diet for 3 months (n=12 animals per
655 group). (**e**) QUICKI and (**f**) mRNA level of *Elovl6* in response to refeeding in gonadal
656 adipose tissue (n=8 animals per group) in C57BL/6J mice fed 60% high fat diet for 3 months
657 (n=8 animals per group). (**g-j**) Experiments were carried out in wild type (WT, white bars)
658 and in mice with zinc finger nuclease-mediated deletion of *Lipe* exon B which promoter
659 drives HSL expression in fat cells (*Lipe*$^{exonB-/-}$, grey bars). (**g**) mRNA levels of transcripts
660 containing different exons encoding HSL in inguinal adipose tissue (n=12 animals per group).
661 **(h)** Western blot analysis of adipose tissue HSL protein content (10 µg total protein) (WT n=7
662 animals; *Lipe*$^{exonB-/-}$ n =5 animals). GAPDH was used as Western blot loading control. Size
663 markers (in kDa) are shown on illustrative Western blot panel. (**i**) Plasma glucose
664 concentration and area under the curve (AUC) during a glucose tolerance test (WT n=7
665 animals, *Lipe*$^{exonB-/-}$ n=5 animals) in mice fed 60% high fat diet for 3 weeks and (**j**) mRNA
666 level of adipose tissue *Elovl6* (WT n=5 animals, *Lipe*$^{exonB-/-}$ n=6 animals). Data are mean
667 ±sem. Statistical analysis was performed using Mann and Whitney's test (**a-c**, **h-j**), unpaired
668 Student's t test (**e-g**) or two-way ANOVA with Bonferroni's post-hoc tests (**d**). Statistical
669 tests were two-sided. *P<0.05 compared to control.
670
671 **Figure 3.** ELOVL6 has a positive effect on insulin signaling in adipocytes. (**a, b**) Experiments
672 were carried out in control (white bars, siCTR), single HSL (grey bars, siHSL), single
673 ELOVL6 (light orange bars, siELOVL6) or dual HSL/ELOVL6-deprived (dark orange bars,
674 siHSL/siELOVL6) hMADS adipocytes in basal (-) and insulin-stimulated (+, 100nM)
675 conditions. Insulin signaling evaluated by activating phosphorylation of IRS1 (pY612) (n=7

biologically independent samples per group) (Insulin stimulation: P=0.0238) (**a**) and AKT (pS473) (n=7 biologically independent samples per group) (Insulin stimulation: P<0.0001) (**b**). (**c**) Insulin signaling evaluated by activating phosphorylation of AKT (pS473) in wild type (WT, white bars, n=4 animals) and *Elovl6* null (*Elovl6*-/-, light orange bars, n=3 animals) mice injected with a bolus of insulin (Insulin stimulation: P<0.0001). Size markers (in kDa) are shown on illustrative Western blot panels. (**d, e**) Plasma glucose concentration during an insulin tolerance test (n=9 animals per group) (**d**) and gonadal adipose tissue *Elovl6* mRNA levels in response to refeeding (**e**) in DBA/2J (white bars, n=6 animals) and C57Bl/6J (light green bars, n=5 animals) mice. (**f, g**) Glucose disposal rate (GDR) (**f**) and mRNA level of *ELOVL6* in visceral adipose tissue (**g**) from lean healthy (LE, white bars, n=13 individuals) and obese women with metabolic syndrome (MS, light red bars, n=15 individuals). (**h, i**) M-value (**h**) and normalized *ELOVL6* mRNA level (**i**) in subcutaneous adipose tissue of obese women before and two years after bariatric surgery (n=14 individuals). Data are mean ±sem. Statistical analysis was performed using paired (**a, b, d**) and unpaired (**c**) two way ANOVA with Bonferroni's post hoc tests, unpaired Student's t test (**f**), Mann and Whitney's test (**e, g**), and Wilcoxon's test (**h, i**). Statistical tests were two-sided. *P<0.05, **P<0.01, ***P<0.001 compared to control condition or other mouse strain. In cell experiments, $^{\$\$}$P<0.01, $^{\$\$\$}$P<0.001 compared to HSL-deprived adipocytes.

Figure 4. Oleic acid content in PL and plasma membrane fluidity mediates ELOVL6 positive effect on insulin signaling. (**a-h**) Experiments were carried out in control (white bars, siCTR), single HSL (grey bars, siHSL), single ELOVL6 (light orange bars, siELOVL6) or dual HSL/ELOVL6-deprived (dark orange bars, siHSL/siELOVL6) hMADS adipocytes. (**a, b**) Fatty acid composition in TG (**a**) and PL (**b**) (n=6 biologically independent samples per group). (**c-f**) hMADS adipocytes were treated with vehicle (DMSO), 1µM of ELOVL6

inhibitor (ELOVL6i) or 75nM of SCD inhibitor (SCDi) for 48h. Fatty acid ratios (n=6 for ELOVL6i and n=5 for SCDi biologically independent samples per group) (**c,e**) and insulin signaling evaluated by activating phosphorylation of AKT (pS473) in basal (-) and insulin-stimulated conditions (+,100nM) (n=4 biologically independent samples per group for ELOVL6i and SCDi) (Insulin stimulation: P<0.0001) (**d,f**). DMSO-treated adipocyte values are common to panels **d** and **f** and, **Supplementary Fig. 1e**. (**g, h**) hMADS were treated with vehicle (V), 100µM (O100) or 500µM (O500) of oleic acid for 48h. Oleic acid levels in PL (n=5 biologically independent samples per group) (**g**) and insulin signaling evaluated by activating phosphorylation of AKT (pS473) (n=5 biologically independent samples per group) in basal (-) or insulin-stimulated (+, 100nM) conditions (Insulin stimulation: P=0.0003) (**h**). For panels **d**, **f** and **h**, cropped images of vehicle and treatment lanes originate from the same blot. Size markers (in kDa) are shown on illustrative Western blot panels. (**i-l**) Experiments were carried out in control hMADS adipocytes expressing green fluorescent protein (GFP) (white bars, Adeno-CTR) or overexpressing human ELOVL6 and GFP (avocado bars, Adeno-ELOVL6). (**i, j**) Fatty acid ratio (n=8 biologically independent samples per group) (**i**) and activating phosphorylation of IRS1 (pY612) in basal (-) and insulin-stimulated conditions (+, 100nM) (n=8 biologically independent samples per group) (Insulin stimulation: P<0.0001) (**j**). (**k, l**) FRAP experiments using fluorescent cholera toxin B (Alexa555-CTxB) (n=5 independent experiments). (**k**) Representative confocal microscope image showing GFP and Alexa455-CTxB at room temperature of a successfully transduced hMADS adipocyte. Scale bar, 50µm. (**l**) Calculated mobile fraction (white bar, n=17 analyzed cells; avocado bar, n=16 analyzed cells). Data are mean ±sem. Statistical analysis was performed using Wilcoxon's test (**a,b**), paired (**c-f**, **h**, **j**) and unpaired (**d**) two way ANOVA with Bonferroni's post hoc tests, Friedman's with Dunn's post hoc tests (**g**), paired Student's t test (**i**) and Mann and Whitney's test (**l**). Statistical tests were two-sided. *P<0.05, **P<0.01, ***P<0.001 compared to control.

$^{\$\$}P<0.01$, $^{\$\$\$}P<0.001$ compared to HSL-deprived adipocytes. $^{\#}P<0.05$, $^{\#\#}P<0.01$ compared to HSL- and ELOVL6-deprived adipocytes.

Figure 5. The glucose-sensitive transcription factor, ChREBP, mediates the beneficial effect of diminished HSL expression on glucose metabolism and insulin signaling in adipocytes. (**a-e**) Experiments were carried out in control (white bars, siCTR), single HSL (grey bars, siHSL), single ChREBP (light brown bars, siChREBP) or dual HSL/ChREBP-deprived (dark brown bars, siHSL/siChREBP) hMADS adipocytes in basal (-) and insulin-stimulated (+, 100nM) conditions. (**a**) Glucose transport using radiolabelled 2-deoxyglucose (n=12 biologically independent samples per group) (Insulin stimulation: P<0.0001). (**b, c**) *de novo* lipogenesis using radiolabelled glucose (n=9 biologically independent samples per group) (Insulin stimulation: P=0.0002) (**b**) or radiolabelled acetate (n=6 biologically independent samples per group) (Insulin stimulation: P=0.0014) (**c**). (**d, e**) Insulin signaling evaluated by activating phosphorylation of IRS1 (pY612) (n=8 biologically independent samples per group) (Insulin stimulation: P=0.0245) (**d**) and AKT (pS473) (n=8 biologically independent samples per group) (Insulin stimulation: P<0.0001) (**e**). Size markers (in kDa) are shown on illustrative Western blot panels. (**f-h**) Experiments were carried out in control (white bars, siCTR) and ChREBP-deprived (light brown bars, siChREBP) hMADS adipocytes. (**f, g**) Fatty acid composition in TG (**f**) and PL (**g**) (n=8 biologically independent samples per group). (**h**) mRNA levels of lipogenic enzymes (n=6 biologically independent samples per group). (**i**) mRNA levels of lipogenic enzymes in inguinal adipose tissue of wild type (WT, white bars, n=7 animals) and *ChREBP* null mice (*Mlxipl*-/-, light brown bars, n=6 animals). (**j,k**) Experiments were carried out in control (white bars, siCTR) and HSL-deprived (grey bars, siHSL) hMADS adipocytes. (**j**) Induction of mRNA levels of *ChREBPα* and *ChREBPβ* (n=8 biologically independent samples per group) and (**k**) ChREBP recruitment on *ELOVL6*

ChoRE (n=3 independent experiments). (**l, m**) Correlations between mRNA levels of *ELOVL6* and *ChREBPβ* in hMADS adipocytes (n=64 biologically independent samples) (**l**) and in human subcutaneous adipose tissue (n=31 individuals) (**m**). (**n, o**) mRNA levels of *ChREBPβ* (n=7 biologically independent samples per group) (**n**) and *ELOVL6* (n=7 biologically independent samples per group) (**o**) in human subcutaneous adipose tissue in basal condition or during hyperglycemic-hyperinsulinemic clamp. Data are mean ±sem. Statistical analysis was performed using paired two way ANOVA with Bonferroni post hoc tests (**a-e**), paired Student's t test (**f, g, j**), Wilcoxon's test (**h, n, o**), Mann and Whitney's test (**i**) and linear regression (**l, m**). Statistical tests were two-sided. *P<0.05, **P<0.01, ***P<0.001 compared to control. $^{\$}$P<0.05, $^{\$\$}$P<0.01, $^{\$\$\$}$P<0.001 compared to HSL-deprived adipocytes. $^{\#}$P<0.05, $^{\#\#}$P<0.01 compared to ChREBP-deprived adipocytes.

Figure 6. HSL inhibits ChREBP activity through protein-protein interaction. (**a**) Representative image of immunocomplexes between immobilized FLAG-ChREBPα and recombinant HSL (Rec.HSL) (n=3 independent experiments). (**b**) Representative surface plasmon resonance assay sensorgram showing the binding of HSL to ChREBP. Purified ChREBP (220RU) was first injected on a sensorchip with immobilized anti-ChREBP antibody. Following ChREBP binding, PR65α (no signal) and HSL (35RU) were consecutively injected (n=3 independent experiments). (**c**) Endogenous interaction between HSL and ChREBP in human adipocytes (n=3 biologically independent samples per group). Anti-ChREBP antibody was used for immunoprecipitation (IP). Normal Rabbit IgG antibody was used as negative control. (**d**) Endogenous interaction between HSL and ChREBP in white adipose tissue of *Lipe*$^{+/-}$ (+/-) and wild type (+/+) mice (n=4 animals per group). Anti-ChREBP antibody was used for immunoprecipitation. Rabbit IgG antibody was used as negative control. β-actin was used as Western blot loading control. (**e**) In situ proximity

776 ligation assays (red signals) performed with anti-HSL and anti-ChREBP antibodies (PLA
777 HSL/ChREBP) and corresponding image under visible light (Phase) in control (siCTR) and
778 HSL-deprived (siHSL) hMADS adipocytes. Nuclei were labelled in blue using DAPI.
779 Representative image (6 independent experiments). Scale bars, 50µm. (**f**) Immunodetection of
780 ChREBP (red) in control (siCTR) and HSL-deprived (siHSL) hMADS adipocytes.
781 Representative image (4 independent experiments). Nuclei were labelled in blue using DAPI.
782 Scale bars, 50µm. (**g**) ChREBPα protein levels in nuclear extracts from control (siCTR) and
783 HSL-deprived (siHSL) hMADS adipocytes (n=8 biologically independent samples per
784 group). (**h**) ChREBPα protein levels in nuclear extracts from white adipose tissue of wild type
785 (WT, n=8 animals) and *Lipe*$^{+/-}$ (n=9 animals) mice. (**i**) Luciferase assays following
786 transfection in HEK-293 cells of carbohydrate-responsive elements (ChoRE) fused to the
787 luciferase gene along with expression vectors for ChREBP and HSL. ChoRE activity was
788 measured in HEK-293 cells transfected with empty plasmid (pcDNA), ChREBP and different
789 concentrations of HSL expression plasmids under low (5mM, G5) (n=6 biologically
790 independent samples per group) and high (25mM, G25) glucose concentrations (n=4
791 biologically independent samples per group). (**j**) HSL and ChREBPα immunocomplexes in
792 HEK-293 cells transfected with empty plasmid (pcDNA3), FLAG-ChREBP, full lengh HSL
793 (HSL) or short form HSL (HSL-S) expression plasmids. Anti-FLAG antibody was used for
794 immunoprecipitation. β-actin was used as Western blot loading control (n=3 independent
795 experiments) (**k,l**) Effect of overexpression of the short inactive form of HSL (HSL-S) in
796 hMADS adipocytes. Experiments were carried out in control (siCTR, white bars) and HSL-
797 deprived (siHSL, grey bars) hMADS adipocytes overexpressing green fluorescent protein
798 (GFP, Ad-CTR) or the short inactive form of HSL (Ad-HSL-S). (**k**) mRNA levels of *ELOVL6*
799 (n=10 biologically independent samples per group). (**l**) Activating phosphorylation of IRS1
800 (pY612) in basal (-) and insulin-stimulated (+, 100nM) conditions (n=6 biologically

801 independent samples per group, Insulin stimulation: P<0.0001). Size markers (in kDa) are
802 shown on illustrative Western blot panels. Data are mean ± sem. Statistical analysis was
803 performed using paired Student's t test (**g**), Mann and Whitney's test (**h**) or paired two-way
804 ANOVA with Bonferroni's post-hoc tests (**i, k, l**). Statistical tests were two-sided. *P<0.05,
805 **P<0.01 ***P<0.001 compared to ChREBP condition (**i**) or control adipocyte (**l**). $^{\$}$P<0.05,
806 $^{\$\$\$}$P<0.001 compared to pcDNA condition (**i**) or siHSL/Ad-CTR adipocytes (**k, l**).
807

METHODS

General experimental approaches. No samples, mice, human research participants and data points were excluded from the reported analysis. Randomization was not performed. Analyses were not blinded except when noted below. Detailed information and description of common techniques are described in Supplementary Methods as indicated below.

Culture of human adipocytes and in vitro measurements.

Culture of adipocytes. hMADS cells were expanded in DMEM 5.5 mM glucose (Lonza) supplemented with 10% fetal bovine serum (Lonza), 2 mM L-glutamine (Invitrogen), 10 mM HEPES buffer (Lonza), 50 units/ml of penicillin (Invitrogen), 50 mg/ml of streptomycin (Invitrogen), supplemented with 2.5 ng/ml of fibroblast growth factor 2 (Sigma). At confluence, fibroblast growth factor 2 was removed from proliferation medium. On the next day (day 0), the cells were incubated in differentiation medium (DMEM/Ham's F-12 medium containing 7.8 mM glucose, HEPES, L-glutamine, penicillin/streptomycin, 10 µg/ml of transferrin (Sigma), 10nM of insulin (Sigma), 0,2 nM triiodothyronine (Sigma), 100 µM 3-isobutyl-1-methylxanthine (Sigma), 1 µM dexamethasone (Sigma), and 100 nM rosiglitazone (Sigma)). At days 3 and 10, respectively, dexamethasone and 3-isobutyl-1-methylxanthine, and then rosiglitazone were removed from culture medium. The experiments were carried out between days 12 and 15.

For primary culture and differentiation of human preadipocytes, subcutaneous adipose tissue samples were obtained from 5 women (age 39 ± 9 years; BMI 28 ± 4 kg/m^2) undergoing elective plastic surgery in the abdominal or dorsal region at Rangueil Hospital, Toulouse, France. Adipose tissue was cleaned from blood vessels and fibrous material, minced into pieces and digested in 1 volume of collagenase I (300 units/ml, Sigma) for 90 min in 37 °C shaking water bath. Digested tissue was filtered through 250 µm strainer, diluted with PBS/gentamycin and centrifuged at 1300 rpm for 5 min. Pellet was incubated in erythrocyte

lysis buffer for 10 min at room temperature. Cells were filtered, centrifuged, resuspended in PM4 medium with 132 nmol/L insulin for differentiation and collected at day 13 [51,52]. The study was approved by the Ethics Committee of Toulouse University Hospitals (Comité de Protection des Personnes Sud Ouest et Outre Mer 2, DC-2014-2039). The volunteers signed informed consent for anonymous use of samples.

HEK293 and HepG2 cell cultures. See Supplementary Methods.

RNA interference. RNA interference was achieved by small interfering RNA (siRNA). Briefly, on day 7 and day 4 of differentiation respectively, hMADS and primary preadipocytes were detached from culture dishes with trypsin/EDTA (Invitrogen) and counted. Control small interfering RNA against Green Fluorescent Protein (siCTR) and gene-specific siRNA for HSL, ChREBP, ELOVL6 and ATGL (Eurogentec) were delivered into adipocytes using a microporator (Invitrogen) with the following parameters: 1,100 V, 20 ms, 1 pulse. The targeted sequences are provided in Supplementary Methods.

Adenoviral infection. Adenoviruses encoding under the control of a cytomegalovirus promoter, ELOVL6 (ADV-207862), the short form of HSL, both in tandem with GFP, or GFP alone (catalog No. 1060) were obtained from Vector Biolabs. Adenoviral particles (multiplicity of infection, 200) were added in the culture medium for 24 hours at day 11-12 of hMADS cell differentiation. Medium was changed and experiments were carried out 48 hours later.

Plasmid transfection. See Supplementary Methods.

Oleic acid supplementation in human adipocytes. See Supplementary Methods.

Treatments with enzyme inhibitors. For FAS, SCD and ELOVL6 inhibition, hMADS adipocytes were respectively treated with 1μM of compound AZ12756122 (ex 117 from WO2008075070A1, synthesized at AstraZeneca), 75nM of A939572 [24] (Tocris Biosciences) and 1w [23] (provided by AstraZeneca) in culture medium for 48 hours. To study the effect of

858 bioactive FA on the induction of ChREBP, cells were treated for 8h with 10µM of triacsin C
859 (Sigma), an inhibitor of acyl-CoA synthase, in the culture medium.
860 Gene expression analysis. See Supplementary Methods.
861 Characterization of human ChREBPβ-specific exon. See Supplementary Methods.
862 Western blot analysis. See Supplementary Methods.
863 Metabolic measurements. Triacylglycerol hydrolase activity was measured on cell extracts [14].
864 For other metabolic measurements, insulin was removed from culture medium the day before
865 the assay. To determine glucose uptake, cells were incubated 50 min at 37°C with or without
866 100 nM insulin. Then, 125 µM of cold 2-deoxy-Dglucose and 0.4 µCi 2-deoxy-D-[^{3}H]
867 glucose (Perkin Elmer) per well were added for 10 min incubation. Culture plates were put on
868 ice and rinsed with 10 mM glucose in ice-cold PBS and then with ice-cold PBS. Cells were
869 scraped in 0.05N NaOH, and radioactive 2-deoxy-D-glucose uptake was measured by liquid
870 scintillation counting of cell lysate. To determine glucose oxidation, cells were incubated for
871 3 h in Krebs Ringer buffer supplemented with 2% BSA, 10 mM HEPES, 2 mM glucose, and
872 1 µCi D-[^{14}C(U)]glucose (PerkinElmer) with or without 100 nM insulin. A 2x2 cm Whatman
873 3M paper was placed on top of each well and soaked with 120 µL NaOH 1N. After
874 incubation, filter-trapped $^{14}CO_2$ was measured by liquid scintillation counting. Medium was
875 acidified with 1M sulfuric acid and medium $^{14}CO_2$ was trapped by benzethonium hydroxide,
876 during 2 h incubation. Benzethonium-trapped $^{14}CO_2$ was measured by liquid scintillation
877 counting. Specific activity was counted and used to determine the quantity of oxidized
878 glucose equivalent. To assess glucose incorporation into FA, cells were then washed twice in
879 PBS and then scraped in STED. Neutral lipids were extracted in methanol/chloroform (1:2).
880 Organic phase was dried under nitrogen and hydrolyzed in 1mL 0.25N NaOH in
881 methanol/chloroform (1:1) for 1 h at 37°C. The solution was neutralized with 500 µL 0.5N
882 HCl in methanol. FAs and glycerol were separated by adding 1.7 mL chloroform, 860 µL

883 water, and 1 mL methanol/chloroform (1:2). Incorporation of ^{14}C into FAs was measured by
884 liquid scintillation counting of the lower phase. Specific activity was counted and used to
885 determine the quantity of incorporated glucose equivalent. *De novo* lipogenesis was also
886 measured using acetic acid-sodium salt-[1-^{14}C] (PerkinElmer). Cells were incubated for 3h in
887 Krebs buffer supplemented with 10mM HEPES, 2mM glucose, 2%BSA and 2µCi/mL of
888 radiolabelled acetate stimulated with or without 100nM insulin. Cells were then washed twice
889 and harvest in PBS/SDS 0.1%. Neutral lipids were extracted in methanol/chloroform (1:2)
890 method. Incorporation of ^{14}C into neutral lipids was measured by liquid scintillation counting
891 of lower phase. Results from metabolic measurements were normalized to total protein
892 content of cell extracts.
893 ELOVL6 activity. Fatty acid elongation activity was measured in crude microsomal extracts
894 from hMADS adipocytes [41]. Briefly, cells were washed with PBS, scraped in 3 ml of ice-cold
895 250m M sucrose, Hepes 20 mM, EDTA 1 mM, pH 7.5 and dounce-homogenized.
896 Homogenate was centrifuged 1000 g at 4°C for 7 min. Supernatant was collected and
897 centrifuged at 2000 g at 4°C for 30 min. Supernatant was collected and centrifuged at 17000 g
898 at 4°C for 1 hour. The resultant pellet was suspended in 50 µl of 100 mM Tris-HCl, pH 7.4
899 and used for fatty acid elongation activity after determination of protein concentration.
900 ELOVL6 activity was essayed by the measurement of [2-^{14}C]malonyl-CoA (Perkin Elmer)
901 incorporation into exogenous palmitoyl-CoA [53]. ELOVL6 inhibitor (1µM of compound 1w [23])
902 was preincubated 30 min at 37°C with microsomal protein before addition of reaction
903 mixture. Incubation was stopped by adding 0.2 ml of 5M KOH, 10% methanol and saponified
904 at 65°C for 1h. Then the samples were cooled and acidified with 0.2 ml of ice-cold 5N HCl
905 and 0.2 ml of ethanol. Free fatty acids were extracted from the mixture three times with 1 ml
906 of hexane, 2% acetic acid. The pooled hexane fractions were dried under nitrogen and after
907 addition of 3 ml of scintillation cocktail, the radioactivity incorporated was counted. Blanks

908 were carried out in parallel reactions incubated without microsomal fractions. ELOVL6
909 activity obtained by subtracting [^{14}C]malonyl-CoA molecules incorporated into fatty acids in
910 the absence of inhibitor to the values in the presence of the ELOVL6 inhibitor.
911 Chromatin immunoprecipitation assays. Human adipocyte cells (10^7 cells per condition) were
912 fixed with 1% formaldehyde for 15 min and quenched with 0.125 M glycine. Chromatin was
913 isolated by the addition of lysis buffer, followed by disruption with a Dounce homogenizer.
914 Lysates were sonicated and the DNA sheared to an average length of 300-500 bp. Genomic
915 DNA (Input) was prepared by treating aliquots of chromatin with RNase, proteinase K and
916 heat for de-crosslinking, followed by ethanol precipitation (Active Motif Inc.). Pellets were
917 resuspended and the resulting DNA was quantified on a NanoDrop spectrophotometer.
918 Extrapolation to the original chromatin volume allowed quantitation of the total chromatin
919 yield. Aliquots of chromatin (30 µg) were precleared with protein A agarose beads
920 (Invitrogen). Genomic DNA regions of interest were isolated using an antibody against
921 ChREBP (Novus, cat# NB400-135). Positive and negative controls were designed by Active
922 Motif Inc. Complexes were washed, eluted from the beads with SDS buffer, and subjected to
923 RNase and proteinase K treatment. Crosslinks were reversed by incubation overnight at 65 C,
924 and ChIP DNA was purified by phenol-chloroform extraction and ethanol precipitation.
925 Quantitative PCR reactions were carried out in triplicate using SYBR Green Supermix (Bio-
926 Rad, Cat # 170-8882) on a CFX Connect™ Real Time PCR system. Positive and negative
927 control sites were tested for each factor as well as the sites of interest. The resulting signals
928 were normalized for primer efficiency by carrying out qPCR for each primer pair using input
929 DNA (pooled unprecipitated genomic DNA from each sample).
930 Cellular subfractionation. Nuclear and cytosolic fractions from hMADS adipocytes were
931 prepared using Nuclear Extract Kit (40010) from Active Motif. Cells were rinsed with PBS
932 and immediately scrapped into 1X Hypotonic Buffer. For adipose tissue, tissues were ground

933 in liquid nitrogen and lysed using the NE-PER nuclear and cytoplasmic extraction reagent kit
934 (Thermoscientific, 78835). Subsequent steps followed the manufacturer's protocol. Anti-
935 histone H3 (4499, Cell Signaling Technology), anti-lamin A/C (4777, Cell Signaling
936 Technology) and α tubulin (T5168, Sigma) antibodies were used to analyze the efficiency of
937 cellular fractionation.
938 Fatty acid composition of TG and PL. Cells were scraped in PBS and then mixed with
939 methanol supplemented with butylated hydroxytoluene (BHT) 0.001%. Lipid extraction was
940 performed with a chloroform/methanol mixture (1:1) and KCl (0.5 M) after centrifugation
941 (2500rpm, 10min). PL and TG were isolated by thin-layer chromatography on silica glass
942 plates (Merck) using petroleum ether/diethyl ether/acetic acid (80:20:1) as the mobile phase.
943 FA methyl esters were generated by transmethylation of the glycerolipids in methanol with 5
944 % acetyl chloride at 60°C for 1 hour, extracted 2 times by isooctane. Analysis was carried out
945 with a gas chromatograph (Shimadzu GC 2100) equipped with a CP-Wax 58 capillary
946 column, 50 m in length, 0.25-mm external diameter and 0.2-µm thickness of the stationary
947 phase (Varian Inc.), with helium 1 mL/min as carrier gas. Programmed temperature
948 vaporization (PTV system) injector and flame ionization detector were used. Results are
949 expressed in percentage of total FA contained in the sample.
950 Fatty acid composition in phospholipid classes. See Supplementary Methods.
951 Measurement of glycerol and NEFA in culture medium. See Supplementary Methods.
952 Fluorescence recovery after photobleaching (FRAP). Cells were labeled for 15 min with
953 1µg/ml Alexa 555-labeled Cholera ToxinSubunit B (CTxB Molecular Probes) at 4°C, then
954 washed three times in chilled medium supplemented with 25 mM HEPES buffer, pH 7.4.
955 LSM780 confocal microscope, equipped with a high sensitive 32 channel GaAsP detectors,
956 operated with Zen Black software, coupled to a DPSS-laser (561 nm, maximum power 20
957 mW) was used for excitation with a detection bandwidth of 571-624 nm (Carl Zeiss). All

958 experiments were done at room temperature (22°C). Cells were observed using a Plan-
959 Apochromat 63X NA 1.4 oil immersion objective, and the pixel dwell was set to the optimal
960 value of 1.92 µs. The fluorescence intensity of three regions of interest of 6.4 µm×3.2 µm was
961 measured: the photobleached area, a region within the cell that was not photobleached to
962 check for overall photobleaching and cell position fluctuation and the background. After 10
963 prebleach scans (one scan every 200 ms) at 1% maximal laser power to determine initial
964 fluorescence intensity, one photobleaching scan was performed at 100% laser power. Post
965 bleach fluorescence recovery was then sampled at 1% laser power for 150 s. FRAP data
966 analysis was done using the method described by Bonneau *et al.* [54].
967 Immunoprecipitation. HEK293T cells were harvested in a lysis buffer containing 3% NaCl
968 5M, 5% TrisHCl 1M (pH 7.5), 1% EDTA 500mM, 1.338% PPiNa and 0.02% NaF,
969 supplemented with 1% Triton X-100 (Sigma), 2% 50X protease inhibitor cocktail (Roche)
970 and 1% 1mM orthovanadate (Sigma). 1 mg of proteins was immunoprecipitated overnight at
971 4°C, with 40µL of anti-FLAG M2 magnetic beads (Sigma). Beads were gently centrifuged for
972 1 min and washed with the lysis buffer before elution in Laemmli buffer.
973 For immunoprecipitation between purified proteins, FLAG-tagged ChREBP was expressed in
974 HEK293T cells. Cells were harvested in lysis buffer described above. 300 µg of proteins was
975 immunoprecipitated overnight at 4°C with 40µL of anti-FLAG M2 magnetic beads. Beads
976 bound with ChREBP were washed with the lysis buffer and incubated with 1 µg of human
977 recombinant HSL (Cayman) in 350 µl of lysis buffer for 3h at 4 °C with gentle rocking. The
978 beads were washed 3 times with lysis buffer.
979 For endogenous co-immunoprecipitation in hMADS adipocytes, cells were lysed for 15min in
980 1X hypotonic buffer (Active Motif) with 4% 25X protease inhibitor cocktail (Roche) and
981 1mM orthovanadate (Sigma). Cell debris and fat was discarded after 12700rpm centrifugation
982 at 4°C for 15min. Preclearing was performed at 4°C for 30min using 50µL protein G and 4µg

control rabbit (2729, Cell Signaling Technology) or mouse (sc-2025, Santa Cruz) IgG. Beads were discarded and supernatants were incubated with 4µg anti-ChREBP (NB400-135, Novus) ou 2µg anti-HSL (sc-74489, Santa Cruz Biotechnology) for 90 min at 4°C. As negative control of immunoprecipitation, 4µg control rabbit (2729, Cell Signaling Technology) or 2µg mouse (sc-2025, Santa Cruz) IgG were used. Protein A/protein G (50:50) magnetic beads were added for 1h at 4°C. Beads were washed in cold PBS with 4% 25X EDTA and 1mM orthovanadate.

For ChREBP immunoprecipitation in mouse white adipose tissue, fat was cut in small pieces and lysed during 2h in 20 mM Tris/HCl, 150 mM NaCl, 0.5% NP-40 and protease/phosphatase inhibitors; pH 8. Following centrifugation at 15000g for 20 min at 4°C, fat layer was removed before collecting the supernatant. For each immunoprecipitation, 0.8 to 1 mg of protein was precleared with 50 µl of Protein A Dynabeads (ThermoFisher) for 1h at 4°C, then incubated overnight at 4°C with 40µl Protein A dynabeads coupled with 5µg Rabbit IgG or ChREBP antibody (Novus). Beads were washed 4 time with lysis buffer prior elution in 2X Laemmli buffer.

In situ proximity ligation assay and immunofluorescence. In situ proximity ligation assay was performed using Duolink In Situ reagents (Sigma). Cells and pieces of subcutaneous adipose tissue were fixed with 4% paraformaldehyde (Sigma) and permeabilized 15 min at room temperature with 0.2% Triton X-100 (Sigma). Incubation of antibodies, ligation of oligodeoxynucleotides and amplification were performed following manufacturer's instructions. The following primary antibodies were incubated overnight at 4°C: anti-HSL (murine antibody, sc-74489, Santa Cruz Biotechnology), anti-ATGL (mouse antibody, NBP2-59390, Novus), anti-AKT (mouse antibody, 2920, Cell Signaling Technology) and anti-ChREBP (rabbit antibody, NB400-135, Novus). The same antibodies were used in immunofluorescence assays. Anti-mouse (Alexa-fluor 488-conjugated, A21202, and Alexa-

fluor 546-conjugated, A10036, Invitrogen) and anti-rabbit (Alexa-fluor 546-conjugated, Invitrogen) secondary antibodies were incubated at 1/300 for 45min. Neutral lipids were stained using Bodipy (4-3922, Life Technologies) for 30min. Nucleus labeling was performed using Hoescht (33342, 5mg/mL, Invitrogen) for 5 min. Confocal microscopy was performed using Zeiss LSM780. Image processing was similar for all conditions. The same settings were applied to entire images.

Surface Plasmon Resonance assays. All binding studies based on surface plasmon resonance technology were performed on BIAcore T200 optical biosensor instrument (GE Healthcare). Immobilization of anti-ChREBP antibody (NB400-135, Novus) was performed by the Fc region to the chip surface using native Protein A sensorchip in PBS-P+ buffer (20mM Phosphate Buffer pH 7.4, 2.7mM Kcl, 137mM NaCl, and 0.05% surfactant P20) (GE Healthcare). Immobilization step were performed at a flow rate of 5 µl/min with a final concentration of 2µg/ml. Total amount of immobilized antibody was 11000-12000RU. Then all injection steps were performed at a flow rate of 20µl/min.Channel Fc1 was used as a reference surface for non-specific binding measurements.

Luciferase activity. See Supplementary Methods.

Animal studies. No randomization and blinding was performed. Animals from several litters were used in each protocol to avoid litter-to-litter variation.

Mouse models. Targeted disruption of the *Lipe* gene and generation of $Lipe^{+/-}$ mice have been described elsewhere [13]. Before euthanasia, mice were fasted for 24h or refed for 18h supplemented with 20% glucose in drinking water. To create transgenic mice with specific deletion of *Lipe* exon B, mRNA coding for zinc finger nucleases targeting specifically HSL (CompoZr™ Custom Zinc Finger Nucleases, CSTZFN-1KT, Sigma) was injected into pronuclei of one-cell embryos from female B6D2/F1 mice. Homozygous mice ($Lipe^{exonB-/-}$

registered as B6D2-*Lipe*^{em1Land} mice) were obtained. Full description of the model will be published elsewhere. The specific inhibitor of HSL (BAY 59-9435) was synthesized by NoValix (Illkirch, France) [55]. Transgenic mice were fed high fat diet (60% or 45% kcal fat, respectively, D12492 and D12451 from Research Diets) for indicated times. In pharmacological studies, C57BL/6J male mice (12-15 weeks-old, Janvier Laboratories) were treated orally with DMSO or HSL inhibitor (70mg/kg once daily) for 11 days. Eight week-old DBA2/J and C57BL6/J male mice (Charles River) were fed high fat diet (60% kcal fat, D12492 from Research Diets) for 6 weeks before sacrifice. Mice were housed and manipulated according to Inserm guidelines and European Directive 2010/63/UE in the local animal care facility (agreements A 31 555 04 and C 31 555 07). Protocols were approved by the French Ministry of Research following review by local ethical committee (CEEA122).

In studies on ChREBP null mice, 10 to 12 week-old male and female *Mlxipl* global knockout mice [56] and wild-type littermates were maintained in a 12-h light/dark cycle with water and chow diet (65% carbohydrate, 11% fat, and 24% protein). For fasting-refeeding experiment, mice were either fasted for 24h (fasted group) or refed for 18h on chow diet and had access to drinking water with 20% glucose, following a 24h fast (Refed group). Mice were housed and manipulated according to Inserm guidelines and European Directive 2010/63/UE in the local animal care facility (agreement A751320). Protocols were approved by the French Ministry of Research following review by local ethical committee (CEEA34).

Mice homozygous for a deletion in *Elovl6* and their wild-type littermates were phenotyped on a C56BL6/J background [57]. The research has been regulated under the Animals (Scientific Procedures) Act 1986 Amendment Regulations 2012 following ethical review by the University of Cambridge Animal Welfare and Ethical Review Body (AWERB).

Gene and protein expression analyses. See Supplementary Methods.

Measurement of fasting glucose and insulin. See Supplementary Methods.

Glucose and insulin tolerance tests and insulin bolus injection. See Supplementary Methods.

Euglycemic-hyperinsulinemic clamp. See Supplementary Methods.

Human research. Nature of the groups was blinded to the investigator performing gene expression experiments.

Women with differing obese and metabolic status. Participating women (lean group mean age 37 ± 16 years; obese with metabolic syndrome group mean age, 49 ± 11 years) were scheduled to have abdominal surgery (laparoscopic or laparotomic cholecystectomy and gastric banding) [58]. During the surgical procedure, samples of visceral adipose tissue were obtained by surgical excision. Euglycemic hyperinsulinemic clamp was performed at rest after an overnight fast. Each subject gave written informed consent and the study was approved by the Ethics Committee of the Third Faculty of Medicine, Charles University, Prague.

Hyperglycemic hyperinsulinemic clamp. The 8 participating men were 23 ± 3 years-old (BMI, 23 ± 2 kg/m^2). The hyperglycemic hyperinsulinemic clamp was a modification of the hyperglycemic method used by Del Prato et al. combined with the original hyperinsulinemic clamp described by Defronzo [59,60]. For hyperglycemia, the objective was to increase plasma glucose 5.5 mmol/l above fasting level by infusing 20% dextrose in two phases: 1) bolus dose to increase glycemia to the desired target and 2) continuous infusion dose adjusted every 5–10 min according to measured plasma glucose to maintain glycemia at the desired target. To obtain hyperinsulinemia, insulin was co-infused at the rate of 75 $mU/m^2 \cdot min$ for 180 min. The study was approved by the Ethics Committee of University of Montreal. The volunteers gave their written consent after being informed of the nature, purpose, and possible risks of the study.

Morbidly obese subjects undergoing bariatric surgery. This cohort has in part been described before [61]. In brief, 14 obese women (BMI>35 kg/m^2; age, 48 ± 9 years) referred to the

hospital for gastric by-pass surgery (Roux-en-Y) were investigated before surgery and 2 years post-operatively. According to self-report, body weight had been stable (± 2 kg) for at least 3 months prior to both investigations. The study was approved by the regional ethics board in Stockholm and registered at clinicaltrials.gov as NCT01785134. Subjects were randomized to omentectomy or not and this was blinded to investigators and patients. Procedure was explained in detail to each women and written informed consent was obtained.

Gene expression analysis. See Supplementary Methods.

Statistical analysis. Results from biological replicates were expressed as mean ± SEM. Statistical analyses were performed using GraphPad Prism (GraphPad Software v.5.0). D'Agostino and Pearson omnibus normality test was used to test normality. Fischer test was used to test for equality of variances. Data were Log transformed when appropriate to reach normality and uniform distribution. Statistical tests were two-sided. Paired or unpaired Student's t tests, Wilcoxon's test and, Mann and Whitney's test were performed to compare two conditions. Paired or unpaired one-way ANOVA and Friedman's tests were performed and followed respectively by Bonferroni's and Dunn's post hoc tests to determine differences between several groups. Paired or unpaired two-way ANOVA with Bonferroni's post hoc tests were used to compare two variables. Linear regression was used to test association between two variables.

Data availability statement. The data that support the plots within this paper and other findings of this study are available from the corresponding author upon reasonable request.

1106 METHODS-ONLY REFERENCES

1107 51. Skurk, T., Ecklebe, S. & Hauner, H. A novel technique to propagate primary human
1108 preadipocytes without loss of differentiation capacity. *Obesity (Silver Spring)* **15**,
1109 2925-2931 (2007).

1110 52. Rossmeislova, L.*, et al.* Weight loss improves the adipogenic capacity of human
1111 preadipocytes and modulates their secretory profile. *Diabetes* **62**, 1990-1995 (2013).

1112 53. Moon, Y.A., Shah, N.A., Mohapatra, S., Warrington, J.A. & Horton, J.D.
1113 Identification of a mammalian long chain fatty acyl elongase regulated by sterol
1114 regulatory element-binding proteins. *J Biol Chem* **276**, 45358-45366 (2001).

1115 54. Bonneau, L.*, et al.* Plasma membrane sterol complexation, generated by filipin,
1116 triggers signaling responses in tobacco cells. *Biochim Biophys Acta* **1798**, 2150-2159
1117 (2010).

1118 55. Langin, D.*, et al.* Adipocyte lipases and defect of lipolysis in human obesity. *Diabetes*
1119 **54**, 3190-3197 (2005).

1120 56. Iizuka, K., Bruick, R.K., Liang, G., Horton, J.D. & Uyeda, K. Deficiency of
1121 carbohydrate response element-binding protein (ChREBP) reduces lipogenesis as well
1122 as glycolysis. *Proc Natl Acad Sci U S A* **101**, 7281-7286 (2004).

1123 57. Tan, C.Y.*, et al.* Brown Adipose Tissue Thermogenic Capacity Is Regulated by
1124 Elovl6. *Cell Rep* **13**, 2039-2047 (2015).

1125 58. Klimcakova, E.*, et al.* Worsening of obesity and metabolic status yields similar
1126 molecular adaptations in human subcutaneous and visceral adipose tissue: decreased
1127 metabolism and increased immune response. *J Clin Endocrinol Metab* **96**, E73-82
1128 (2011).

1129 59. DeFronzo, R.A., Tobin, J.D. & Andres, R. Glucose clamp technique: a method for
1130 quantifying insulin secretion and resistance. *Am J Physiol* **237**, E214-223 (1979).

60. Del Prato, S.*, et al.* Characterization of cellular defects of insulin action in type 2 (non-insulin-dependent) diabetes mellitus. *J Clin Invest* **91**, 484-494 (1993).

61. Dahlman, I.*, et al.* The fat cell epigenetic signature in post-obese women is characterized by global hypomethylation and differential DNA methylation of adipogenesis genes. *Int J Obes (Lond)* **39**, 910-919 (2015).

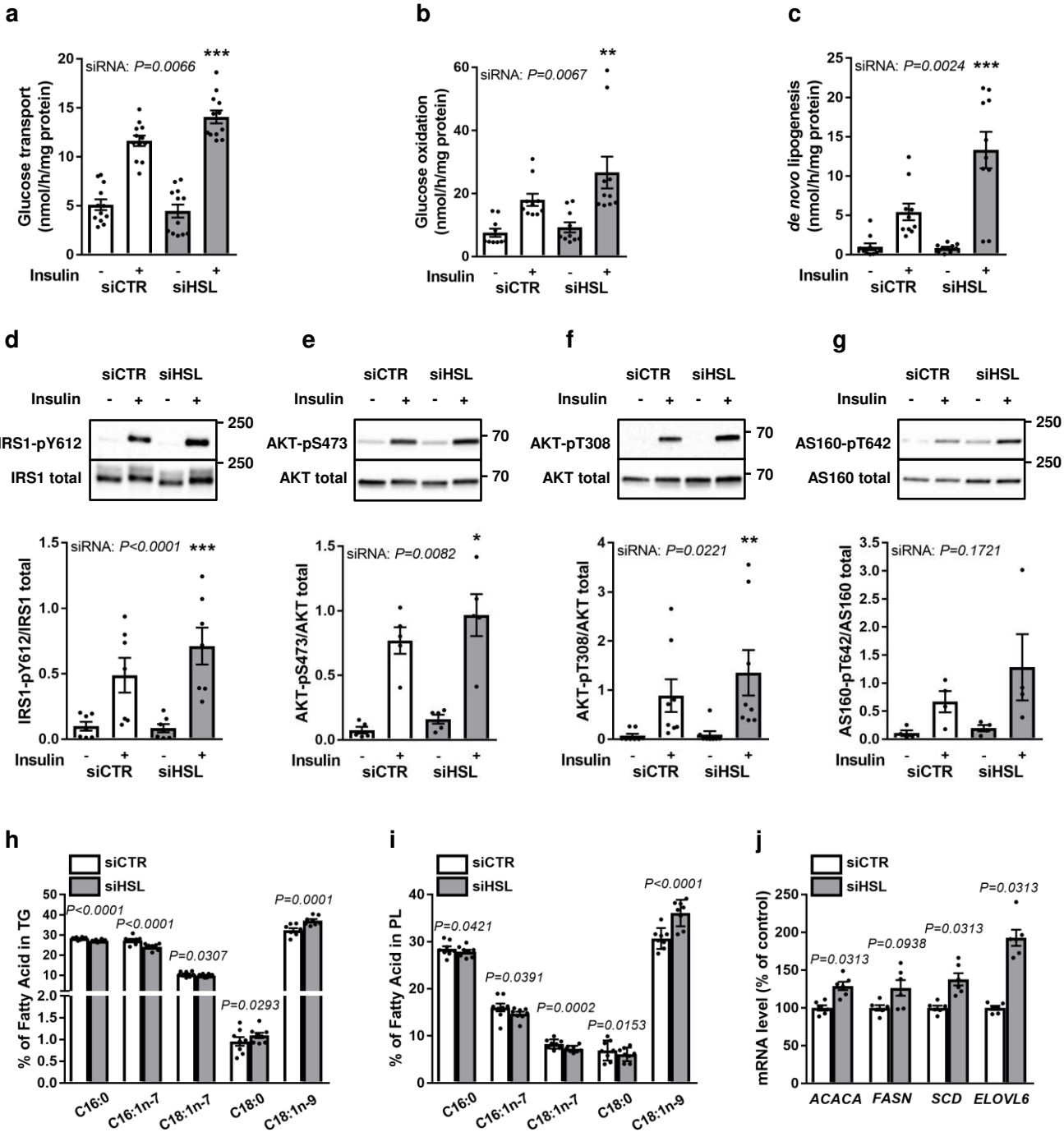
a
Glucose transport (nmol/h/mg protein)
siRNA: P=0.0066
***
Insulin
siCTR
siHSL
b
Glucose oxidation (nmol/h/mg protein)
siRNA: P=0.0067
**
c
de novo lipogenesis (nmol/h/mg protein)
siRNA: P=0.0024
***
d
IRS1-pY612
IRS1 total
IRS1-pY612/IRS1 total
siRNA: P<0.0001
***
e
AKT-pS473
AKT total
AKT-pS473/AKT total
siRNA: P=0.0082
*
f
AKT-pT308
AKT total
AKT-pT308/AKT total
siRNA: P=0.0221
**
g
AS160-pT642
AS160 total
AS160-pT642/AS160 total
siRNA: P=0.1721
h
% of Fatty Acid in TG
P<0.0001
P<0.0001
P=0.0307
P=0.0293
P=0.0001
C16:0
C16:1n-7
C18:1n-7
C18:0
C18:1n-9
i
% of Fatty Acid in PL
P=0.0421
P=0.0391
P=0.0002
P=0.0153
P<0.0001
j
mRNA level (% of control)
P=0.0313
P=0.0938
P=0.0313
P=0.0313
ACACA
FASN
SCD
ELOVL6

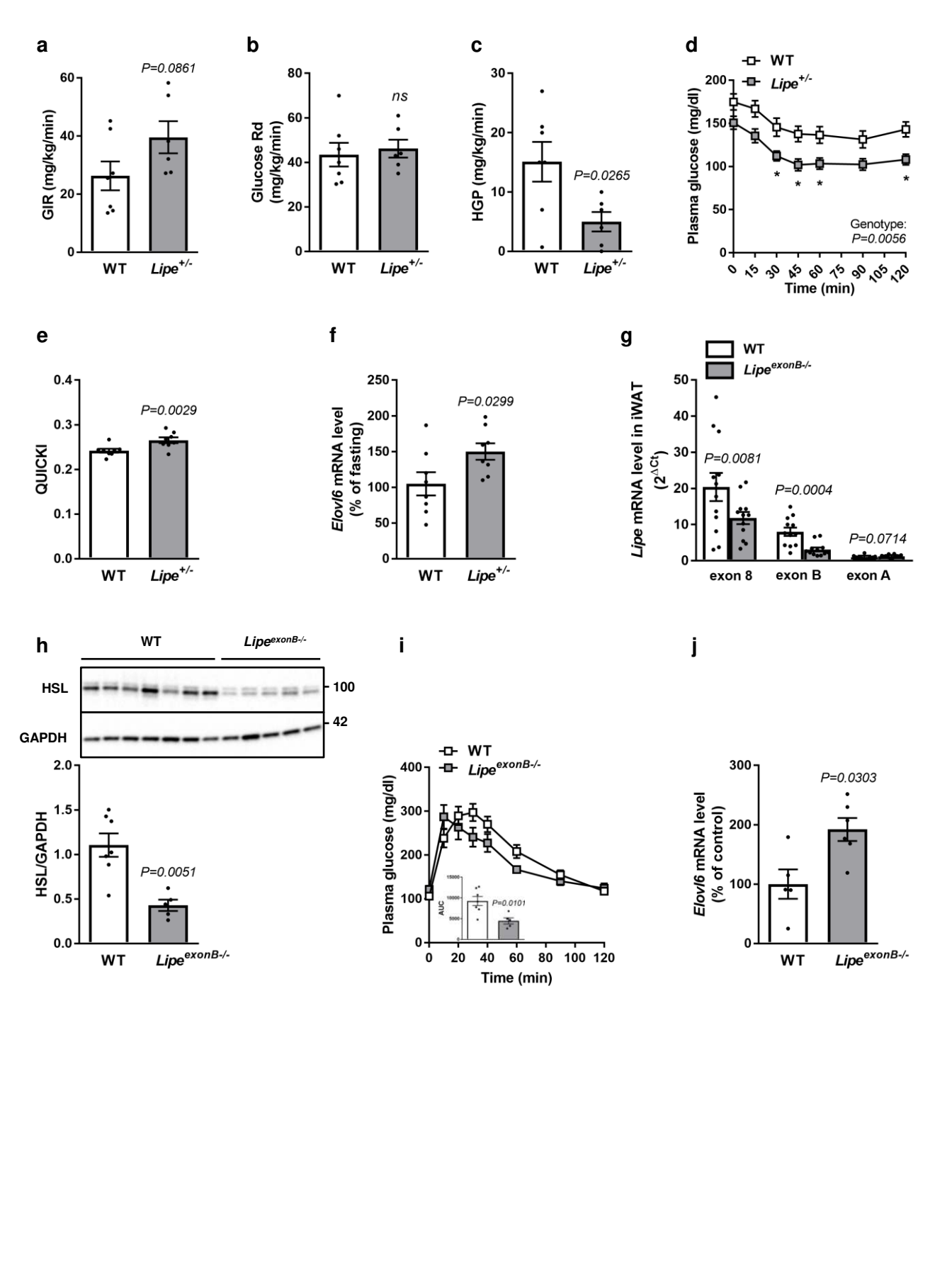
a
GIR (mg/kg/min)
P=0.0861
WT
Lipe+/-
b
Glucose Rd (mg/kg/min)
ns
c
HGP (mg/kg/min)
P=0.0265
d
WT
Lipe+/-
Plasma glucose (mg/dl)
Genotype: P=0.0056
Time (min)
e
QUICKI
P=0.0029
f
Elovl6 mRNA level (% of fasting)
P=0.0299
g
WT
Lipe exonB-/-
Lipe mRNA level in iWAT (2^ΔCt)
P=0.0081
P=0.0004
P=0.0714
exon 8
exon B
exon A
h
WT
Lipe exonB-/-
HSL
GAPDH
100
42
HSL/GAPDH
P=0.0051
i
Plasma glucose (mg/dl)
AUC
P=0.0101
Time (min)
j
Elovl6 mRNA level (% of control)
P=0.0303

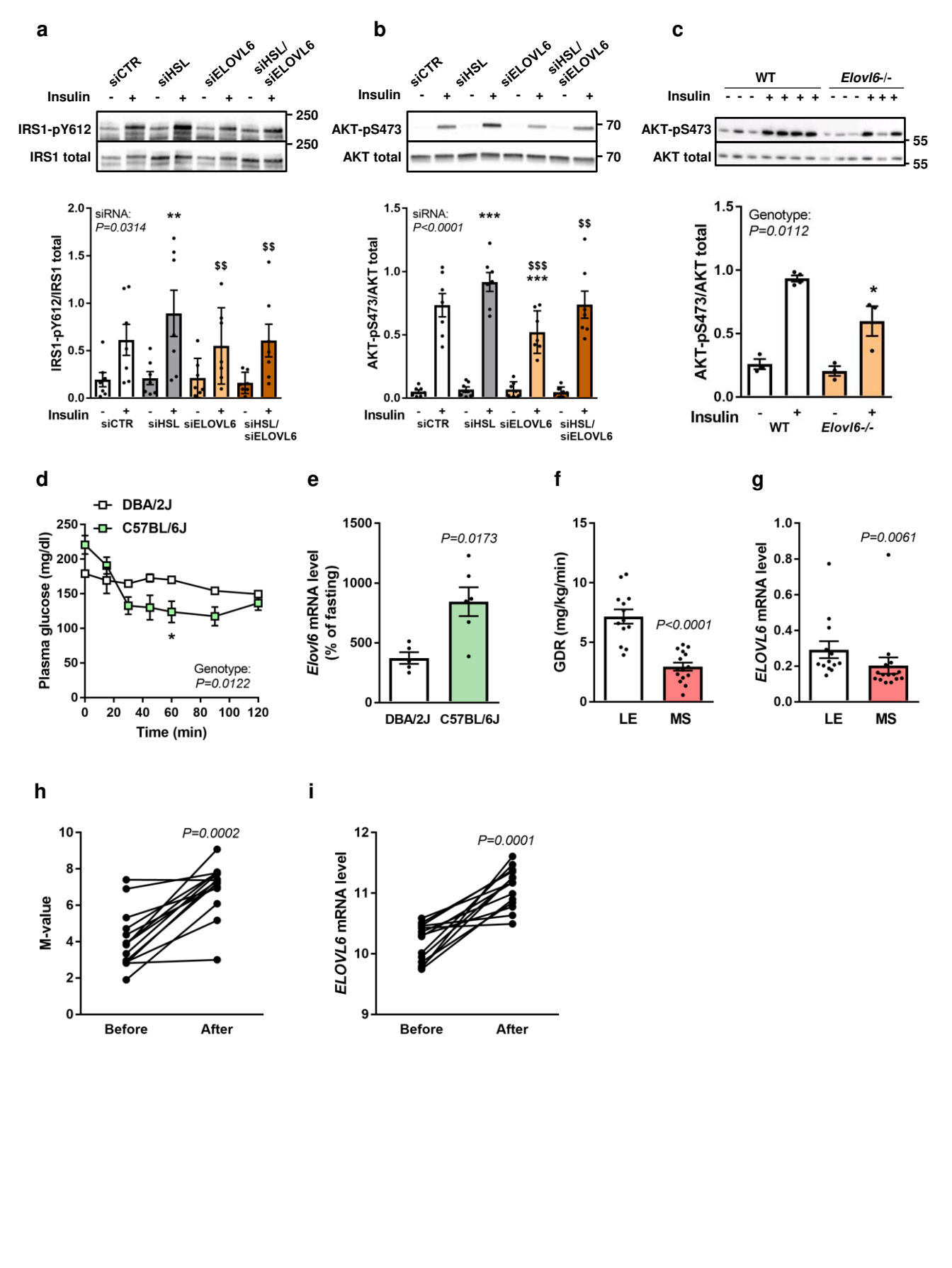
a
siCTR
siHSL
siELOVL6
siHSL/ siELOVL6
Insulin
IRS1-pY612
IRS1 total
250
250
IRS1-pY612/IRS1 total
siRNA:
P=0.0314
siCTR
siHSL
siELOVL6
siHSL/ siELOVL6
b
AKT-pS473
AKT total
70
70
AKT-pS473/AKT total
siRNA:
P<0.0001
c
WT
Elovl6-/-
AKT-pS473
AKT total
55
55
Genotype:
P=0.0112
d
DBA/2J
C57BL/6J
Plasma glucose (mg/dl)
Time (min)
Genotype:
P=0.0122
e
Elovl6 mRNA level
(% of fasting)
P=0.0173
DBA/2J
C57BL/6J
f
GDR (mg/kg/min)
P<0.0001
LE
MS
g
ELOVL6 mRNA level
P=0.0061
LE
MS
h
M-value
P=0.0002
Before
After
i
ELOVL6 mRNA level
P=0.0001
Before
After

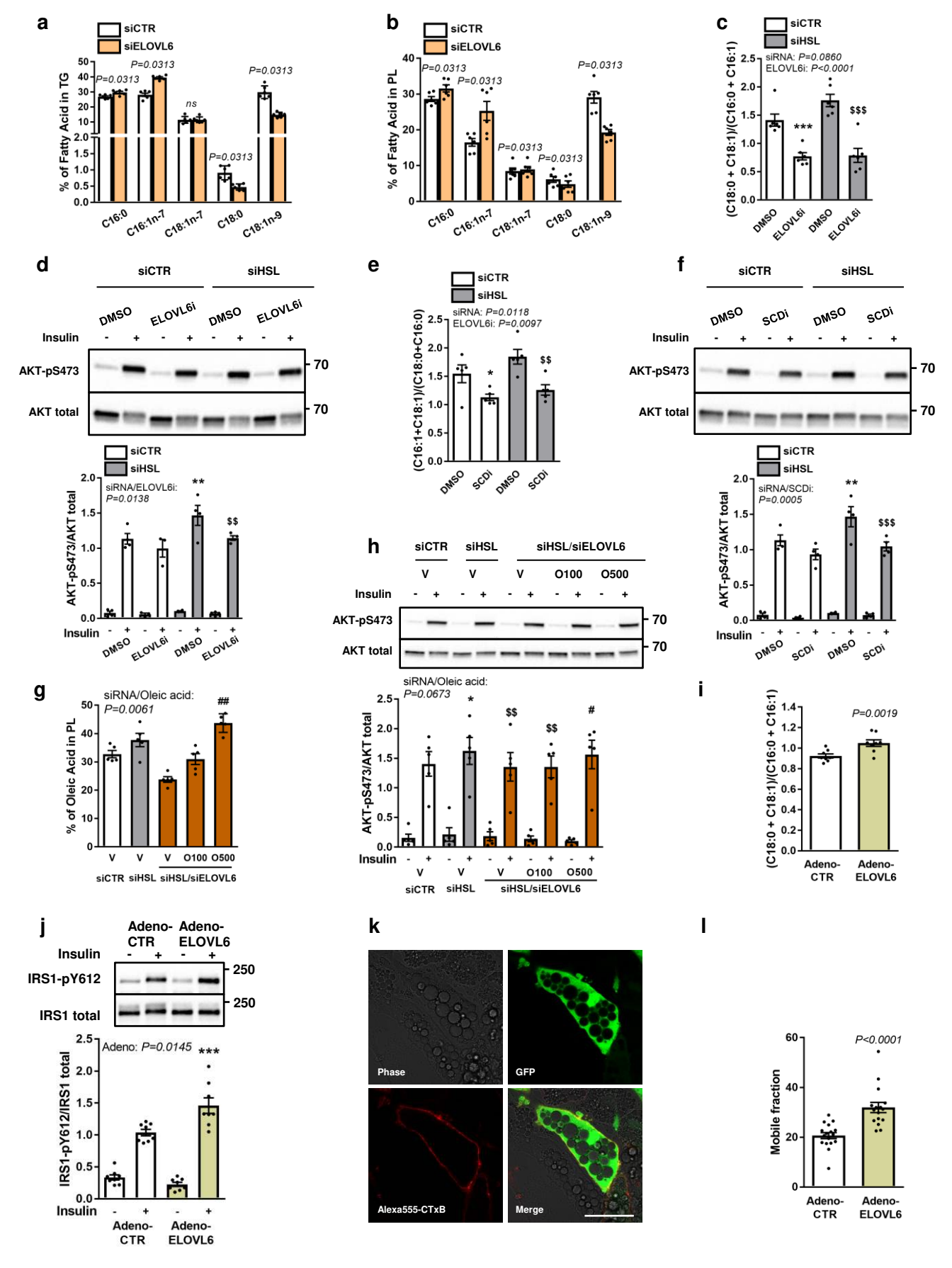
a
siCTR
siELOVL6
% of Fatty Acid in TG
P=0.0313
P=0.0313
ns
P=0.0313
P=0.0313
C16:0
C16:1n-7
C18:1n-7
C18:0
C18:1n-9
b
siCTR
siELOVL6
% of Fatty Acid in PL
P=0.0313
P=0.0313
P=0.0313
P=0.0313
P=0.0313
C16:0
C16:1n-7
C18:1n-7
C18:0
C18:1n-9
c
siCTR
siHSL
siRNA: P=0.0860
ELOVL6i: P<0.0001
(C18:0 + C18:1)/(C16:0 + C16:1)
***
$$$
DMSO
ELOVL6i
DMSO
ELOVL6i
d
siCTR
siHSL
DMSO
ELOVL6i
DMSO
ELOVL6i
Insulin
AKT-pS473
AKT total
70
70
siCTR
siHSL
siRNA/ELOVL6i:
P=0.0138
AKT-pS473/AKT total
**
$$
Insulin
DMSO
ELOVL6i
DMSO
ELOVL6i
e
siCTR
siHSL
siRNA: P=0.0118
ELOVL6i: P=0.0097
(C16:1+C18:1)/(C18:0+C16:0)
*
$$
DMSO
SCDi
DMSO
SCDi
f
siCTR
siHSL
DMSO
SCDi
DMSO
SCDi
Insulin
AKT-pS473
AKT total
70
70
siCTR
siHSL
siRNA/SCDi:
P=0.0005
AKT-pS473/AKT total
**
$$$
Insulin
DMSO
SCDi
DMSO
SCDi
g
siRNA/Oleic acid:
P=0.0061
##
% of Oleic Acid in PL
V
V
V
O100
O500
siCTR
siHSL
siHSL/siELOVL6
h
siCTR
siHSL
siHSL/siELOVL6
V
V
V
O100
O500
Insulin
AKT-pS473
AKT total
70
70
siRNA/Oleic acid:
P=0.0673
*
$$
$$
#
AKT-pS473/AKT total
Insulin
V
V
V
O100
O500
siCTR
siHSL
siHSL/siELOVL6
i
P=0.0019
(C18:0 + C18:1)/(C16:0 + C16:1)
Adeno-CTR
Adeno-ELOVL6
j
Adeno-CTR
Adeno-ELOVL6
Insulin
IRS1-pY612
IRS1 total
250
250
Adeno: P=0.0145
***
IRS1-pY612/IRS1 total
Insulin
Adeno-CTR
Adeno-ELOVL6
k
Phase
GFP
Alexa555-CTxB
Merge
l
P<0.0001
Mobile fraction
Adeno-CTR
Adeno-ELOVL6

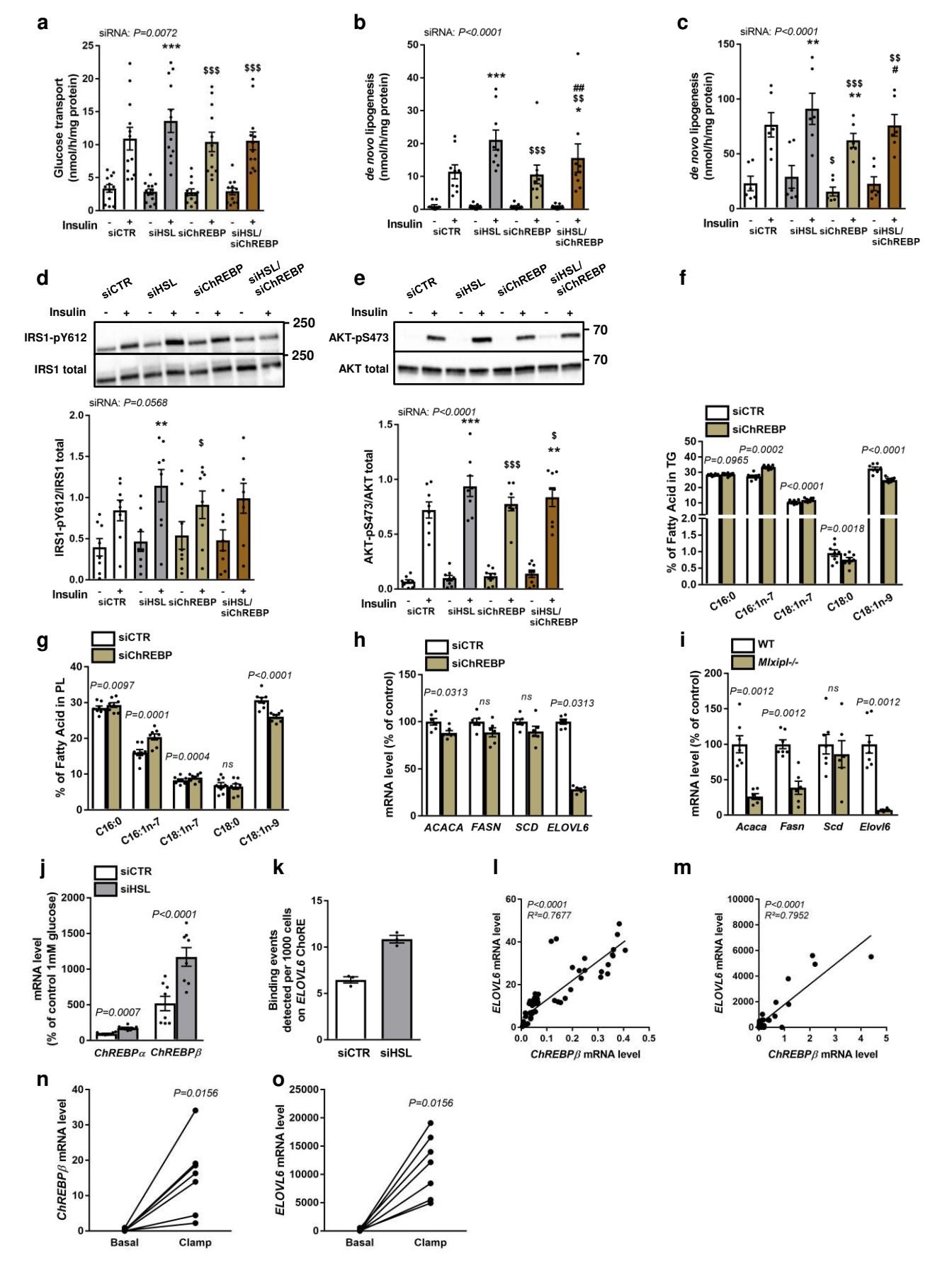
a
siRNA: P=0.0072
Glucose transport (nmol/h/mg protein)
Insulin
siCTR
siHSL
siChREBP
siHSL/ siChREBP
b
siRNA: P<0.0001
de novo lipogenesis (nmol/h/mg protein)
c
siRNA: P<0.0001
de novo lipogenesis (nmol/h/mg protein)
d
IRS1-pY612
IRS1 total
siRNA: P=0.0568
IRS1-pY612/IRS1 total
e
AKT-pS473
AKT total
siRNA: P<0.0001
AKT-pS473/AKT total
f
siCTR
siChREBP
% of Fatty Acid in TG
P=0.0965
P=0.0002
P<0.0001
P=0.0018
P<0.0001
C16:0
C16:1n-7
C18:1n-7
C18:0
C18:1n-9
g
siCTR
siChREBP
% of Fatty Acid in PL
P=0.0097
P=0.0001
P=0.0004
ns
P<0.0001
h
siCTR
siChREBP
mRNA level (% of control)
P=0.0313
ns
ns
P=0.0313
ACACA
FASN
SCD
ELOVL6
i
WT
Mlxipl-/-
mRNA level (% of control)
P=0.0012
P=0.0012
ns
P=0.0012
Acaca
Fasn
Scd
Elovl6
j
siCTR
siHSL
mRNA level (% of control 1mM glucose)
P<0.0001
P=0.0007
ChREBPα
ChREBPβ
k
Binding events detected per 1000 cells on ELOVL6 ChoRE
siCTR
siHSL
l
P<0.0001
R²=0.7677
ELOVL6 mRNA level
ChREBPβ mRNA level
m
P<0.0001
R²=0.7952
ELOVL6 mRNA level
ChREBPβ mRNA level
n
P=0.0156
ChREBPβ mRNA level
Basal
Clamp
o
P=0.0156
ELOVL6 mRNA level
Basal
Clamp

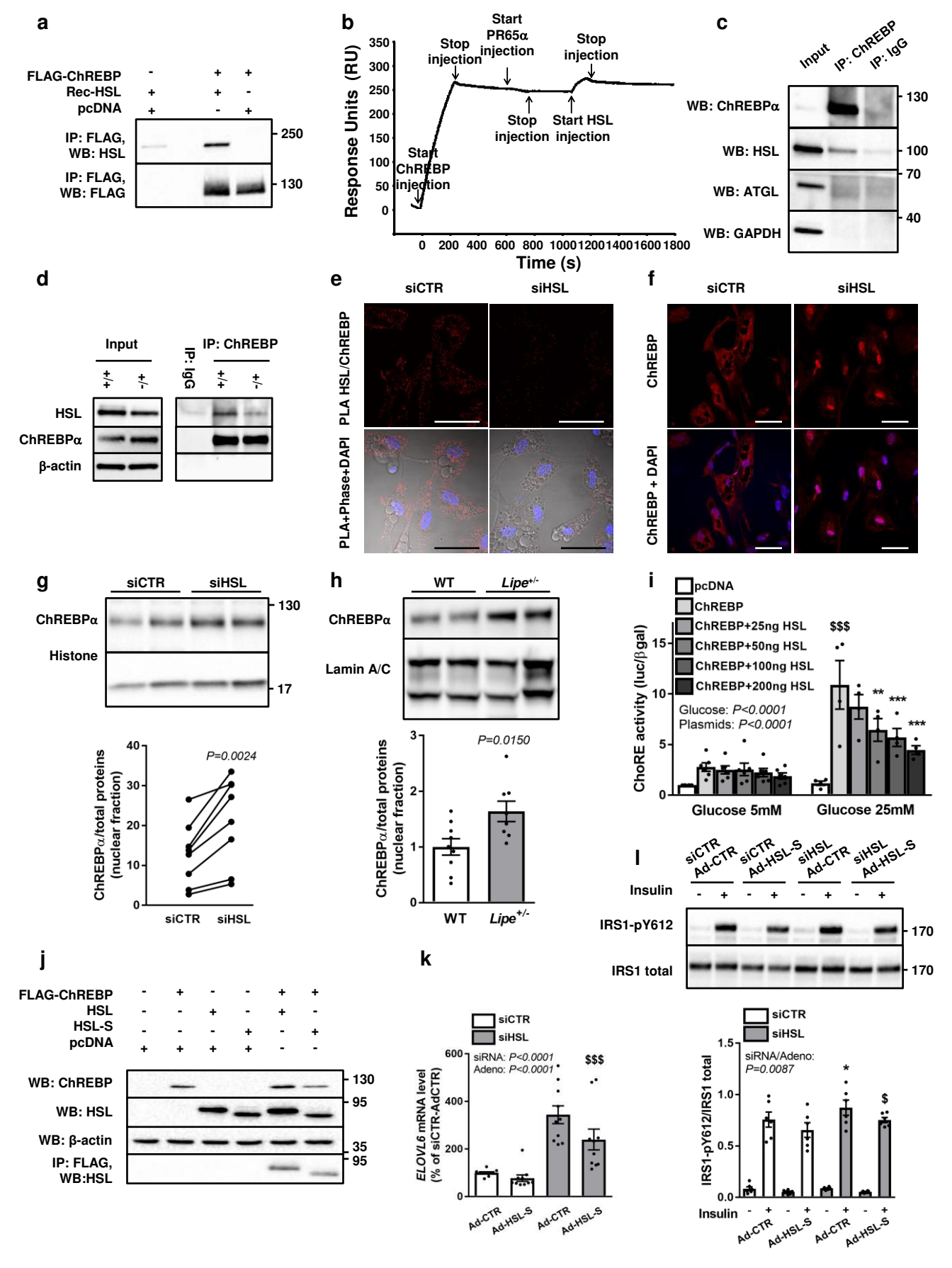
a
FLAG-ChREBP
Rec-HSL
pcDNA
IP: FLAG, WB: HSL
IP: FLAG, WB: FLAG
250
130
b
Response Units (RU)
Time (s)
Start ChREBP injection
Stop injection
Start PR65α injection
Stop injection
Stop injection
Start HSL injection
c
Input
IP: ChREBP
IP: IgG
WB: ChREBPα
WB: HSL
WB: ATGL
WB: GAPDH
d
Input
IP: ChREBP
IP: IgG
HSL
ChREBPα
β-actin
e
siCTR
siHSL
PLA HSL/ChREBP
PLA+Phase+DAPI
f
siCTR
siHSL
ChREBP
ChREBP + DAPI
g
siCTR
siHSL
ChREBPα
Histone
ChREBPα/total proteins (nuclear fraction)
P=0.0024
h
WT
Lipe+/-
ChREBPα
Lamin A/C
P=0.0150
i
pcDNA
ChREBP
ChREBP+25ng HSL
ChREBP+50ng HSL
ChREBP+100ng HSL
ChREBP+200ng HSL
Glucose: P<0.0001
Plasmids: P<0.0001
ChoRE activity (luc/βgal)
Glucose 5mM
Glucose 25mM
l
siCTR Ad-CTR
siCTR Ad-HSL-S
siHSL Ad-CTR
siHSL Ad-HSL-S
Insulin
IRS1-pY612
IRS1 total
j
FLAG-ChREBP
HSL
HSL-S
pcDNA
WB: ChREBP
WB: HSL
WB: β-actin
IP: FLAG, WB:HSL
k
siCTR
siHSL
ELOVL6 mRNA level (% of siCTR-AdCTR)
siRNA: P<0.0001
Adeno: P<0.0001
siRNA/Adeno: P=0.0087
IRS1-pY612/IRS1 total
Ad-CTR
Ad-HSL-S